Cosmology An Introduction

Ricardo Chávez Murillo

Instituto de Radioastronomía y Astrofísica
Universidad Nacional Autónoma de México
October 2020

Contents

Preface

The terms 'cosmological constant', 'dark energy' and 'modified gravity' have been remainders of our incomplete understanding of the "physical reality". Our comprehension has been hampered by incomplete and biased data sets and the consequent theoretical over charged speculation.

Knowledge is constructed progressively, harsh and lengthy battles between proud theoretical systems, between judgements, must be fought before a glimpse of certainty can be acquired. However, sometimes an apparently tractable *petit* problem has been enough to demolish the noblest system.

The cosmic acceleration, detected at the end of the 1990s, could be one of this class of problems that are the key to a new view of reality. First of all, this problem is related to many fields in physics, crossing from gravitation to quantum field theory and to the unknown in the embodiment of quantum gravity with its multiple flavours (e.g. string theory, loop quantum gravity, twistor theory, ...). Even more, the quest for a theoretical account of the observed acceleration has given an enormous impetus to the search for alternative theories of gravity.

The theoretical explanations for the cosmic acceleration are many and diverse, first of all we have the cosmological constant as a form of vacuum energy, then we are faced with a multitude of models in which its origin is explained by means of a substance with an exotic equation of state, and finally we encounter explanations based on modifications of the theory of general relativity.

The fact is that the current empirical data is not enough to discriminate between the great number of theoretical models, and therefore if we want to eventually decide on which is the best model we will need more and accurate data.

List of Symbols

We have attempted to keep the basic notation as standard as possible. In general, the notation is defined at its first occurrence in the text. The signature of the metric is assumed to be $(+,-,-,-)$ and the speed of light, c, is taken to be equal to 1 throughout this work, unless otherwise specified. Throughout this work the Einstein summation convention is assumed. Note that throughout this work the subscript 0 denotes a parameter's present epoch value, unless otherwise specified.

$\Box$	The D'Alembert operator.
χ	The comoving distance.
χ^2	The Chi-square merit function.
δ_k	The perturbations to the mass-energy density decomposed into their Fourier modes.
Γ^a_{bc}	The metric connection coefficients or Christoffel symbols.
κ	The Einstein's gravitational constant.
Λ	The cosmological constant.
$\mathcal{L}$	The Lagrangian density or the likelihood estimator.
μ	The distance modulus.
Ω	The mass-energy density nomarlized to the present ρ_c value.
ρ	The mass-energy density.
ρ_c	The critical density (that required for the Universe to have a flat spatial geometry).
σ	The velocity dispersion from the emission-line width.
$a(t)$	The cosmic scale factor.
c_s	The sound speed.

D_A	The angular distance.
D_L	The luminosity distance.
D_M	The proper distance.
dV	The comoving volume element.
f	The flux.
$G_{\mu\nu}$	The Einstein tensor.
$g_{\mu\nu}$	The metric.
H	The Hubble parameter.
h	The dimensionless Hubble parameter.
L	The luminosity.
M_z	The H II galaxies distance indicator.
p	The pressure.
$q(t)$	The deceleration parameter .
R	The Ricci scalar.
$R_{\mu\nu}$	The Ricci tensor.
R_{curv}	The curvature radius.
R_c	The core radius.
S	The action.
s	The scale of acoustic oscillations.
$t(z)$	The cosmological time.
$T_{\mu\nu}$	The stress-energy tensor.
EW, W	The line equivalent width.
w	The equation of state parameter.
z	The redshift.

Chapter 1

Introduction

"Begin at the beginning," the King said gravely,
"and go on till you come to the end: then stop."
— L. Carroll, Alice in Wonderland

OUR current understanding of the cosmological evidence shows that our Universe is homogeneous on the large-scale, spatially flat and in accelerated expansion; it is composed of baryons, some sort of cold dark matter and a component which acts as having a negative pressure (dubbed 'dark energy' or 'cosmological constant'). The Universe underwent an inflationary infancy of extremely rapid growth, followed by a phase of gentler expansion driven initially by its relativistic and then by its non-relativistic contents but by now its evolution is governed by the dark energy component (e.g. Ratra & Vogeley, 2008; Frieman, Turner & Huterer, 2008).

The observational evidence for dark energy was presented in 1998 when two teams studying type Ia supernovae (SNe Ia), the *Supernova Cosmology Project* and the *High-z Supernova Search*, found independently that these objects were further away than expected in a Universe without a cosmological constant (Riess et al., 1998; Perlmutter et al., 1999). Since then measurements of cosmic microwave background (CMB) anisotropy (e.g. Jaffe et al., 2001; Pryke et al., 2002; Spergel et al., 2007; Planck Collaboration et al., 2013) and of large-scale structure (LSS) (e.g. Tegmark et al., 2004; Seljak et al., 2005), in combination with independent Hubble relation measurements (Freedman et al., 2001), have confirmed the accelerated expansion of the Universe.

The accumulated evidence implies that nearly 70% of the total mass-energy of the Universe is composed of this mysterious dark energy; for which its nature is still largely unknown. Possible candidates of the cause of the accelerated expansion are Einstein's cosmological constant, which implies that the dark energy component is constant in time and uniform in space (Carroll, 2001); or it could be that the dark energy is an exotic form of matter with a time dependent equation of state (e.g. Peebles & Ratra, 2003; Copeland,

Sami & Tsujikawa, 2006); or since the range of validity of General Relativity (GR) is limited, an extended gravitational theory is needed (e.g. Joyce et al., 2014).

From the previous discussion we can see that understanding the nature of dark energy is of paramount importance and it could have deep implications for fundamental physics; it is thus of no surprise that this problem has been called out prominently in recent policy reports (Albrecht et al., 2006; Peacock et al., 2006) where extensive experimental programs to explore dark energy have been put forward.

To the present day, the cosmic acceleration has been traced directly only by means of SNe Ia and at redshifts, $z \sim 1$, a fact which implies that it is of great importance to use alternative geometrical probes at higher redshifts in order to verify the SNe Ia results and to obtain more stringent constrains in the cosmological parameters solution space, with the final aim of discriminating among the various theoretical alternatives that attempt to explain the accelerated expansion of the Universe (cf. Suyu et al., 2012).

Chapter 2

The Expanding Universe

We are to admit no more causes of natural things than such as are both true and sufficient to explain their appearances.

— I. Newton, Rules of Reasoning in Philosophy : Rule I

THE current accepted cosmological model explains the history of the Universe as a succession of epochs characterised by their expansion rates. The Universe expansion rate has changed as one of its energy components dominates over all others. Near the beginning of time around 10^{-36} seconds after the 'big bang', the dominant component is the so called 'inflaton' field and the Universe expands exponentially, then after a reheating process, the dominant component is radiation followed by dark matter and at those epochs the expansion of the universe decelerates. Now the Universe is again in a phase of accelerated expansion and we call 'dark energy' the dominant component that causes it.

Our growing comprehension of the expanding Universe picture has advanced as new data has been accumulating through the technological improvements that have revolutionised astronomy during the past century. The first glimpse of the Universe expansion was obtained using ground based optical spectroscopy (Hubble, 1929), now the available data spans essentially all the electromagnetic spectrum, all kinds of astronomical techniques and is obtained through ground as well as space borne observations.

Through time different tracers have been used to measure the expansion rate, initially extragalactic Cepheids, now Supernovae Ia (SNe Ia), the Cosmic Microwave Background (CMB) and also galaxies. Even so, our current knowledge is insufficient to determine the nature of 'dark energy'.

The cause of the cosmic acceleration is one of the most intriguing problems in all physics. In one form or another it is related to gravitation, high energy physics, extra dimensions, quantum field theory and even more exotic areas of physics, as quantum gravity

or worm holes. However, we still know very little regarding the mechanism that drives the accelerated expansion of the Universe.

With the recent confirmation of the existence of the Higgs boson, the plot thickens even more. The electroweak phase transition generated by the Higgs potential induces a non vanishing contribution to the vacuum energy at the classical level that is blatantly in discordance with the accepted value for the cosmological constant in the 'concordance' (ΛCDM) cosmological model, thus leaving us with an embarrassingly large fine tuning problem (cf. Solà, 2013).

Due to the lack of a fundamental physical theory explaining the accelerated expansion, there have been many theoretical speculations about the nature of dark energy (e.g. Caldwell & Kamionkowski, 2009; Frieman, Turner & Huterer, 2008); furthermore and most importantly, the current observational/experimental data is not adequate to distinguish between the many adversary theoretical models.

Essentially one can probe dark energy by one or more of the following methods:

- Geometrical probes of the cosmic expansion, which are directly related to the metric like distances and volumes.

- Growth probes related to the growth rate of the matter density perturbations.

The existence of dark energy was first inferred from a geometrical probe, the redshift-distance relation of SNe Ia (Riess et al., 1998; Perlmutter et al., 1999); this method continues to be the preeminent way to probe directly the cosmic acceleration. The recent *Union2.1* (Suzuki et al., 2012), *SNLS3* (Conley et al., 2011) and *PS1* (Rest et al., 2013) compilations of SNe Ia data are consistent with a cosmological constant, although the results, within reasonable statistical uncertainty, also agree with many dynamical dark-energy models (Shafer & Huterer, 2014). It is therefore of great importance to trace the Hubble function to higher redshifts than currently probed, since at higher redshifts the different models deviate significantly from each other (Plionis et al., 2011).

In this chapter we will explore the Cosmic Acceleration issue; the first section is devoted to a general account of the basics of theoretical and observational cosmology, in the second section we present a brief outlook of the observational evidence which supports the cosmic acceleration; later we will survey some of the theoretical explanations of the accelerating expansion and finally we will overview some probes used to test the Universe expansion.

Finally, a few words of caution regarding the terminology used. Through this chapter we will be using the term *dark energy* as opposed to *cosmological constant*, in the sense of a time-evolving cause of the cosmic acceleration. However, in later chapters we will use only the term *dark energy* since we consider it as the most general model, of which the *cosmological constant* is (mathematically) a particular case, while it effectively reproduces also the phenomenology of some modified gravity models.

2.1 Cosmology Basics

The fundamental assumption over which our current understanding of the Universe is constructed is known as the cosmological principle, which states that the Universe is homogeneous and isotropic on large-scales. The evidences that sustain the cosmological principle are basically the near-uniformity of the CMB temperature (e.g. Spergel et al., 2003) and the large-scale distribution of galaxies (e.g. Yadav et al., 2005).

Under the assumption of homogeneity and isotropy, the geometrical properties of space-time are described by the Friedmann-Robertson-Walker (FRW) metric (Robertson, 1935), given by

$$ds^2 = dt^2 - a^2(t)\left[\frac{dr^2}{1-kr^2} + r^2(d\theta^2 + \sin^2\theta d\phi^2)\right], \tag{2.1}$$

where r, θ, ϕ are spatial comoving coordinates (i.e., where a freely falling particle comes to rest) and t is the time parameter, whereas $a(t)$ is the cosmic scale factor which at the present epoch, t_0, has a value $a(t_0) = 1$; k is the curvature of the space, such that $k = 0$ corresponds to a spatially flat Universe, $k = 1$ to a positive curvature (three-sphere) and $k = -1$ to a negative curvature (saddle as a 2-D analogue). Note that we are using units where the speed of light, $c = 1$.

From the FRW metric we can derive the cosmological redshift, i.e. the amount that a photon's wavelength (λ) increases due to the scaling of the photon's energy with $a(t)$, with corresponding definition:

$$1 + z \equiv \frac{\lambda_0}{\lambda_e} = \frac{a(t_0)}{a(t)} = \frac{1}{a(t)}, \tag{2.2}$$

where, z is the redshift, λ_0 is the observer's frame wavelength and λ_e is the emission's frame wavelength. Note that throughout this thesis the subscript 0 denotes a parameter's present epoch value.

In order to determine the dynamics of the space-time geometry we must solve the GR field equations for the FRW metric, in the presence of matter, obtaining the cosmological field equations or Friedmann-Lemaître equations (for a full derivation see Appendix A):

$$\left(\frac{\dot{a}}{a}\right)^2 = \frac{8\pi G\rho}{3} - \frac{k}{a^2} + \frac{\Lambda}{3}, \tag{2.3}$$

$$\frac{\ddot{a}}{a} = -\frac{4\pi G}{3}(\rho + 3p) + \frac{\Lambda}{3}, \tag{2.4}$$

where ρ is the total energy density of the Universe, p is the total pressure and Λ is the cosmological constant.

In eq.(2.3) we can define the Hubble parameter

$$H \equiv \frac{\dot{a}}{a}, \tag{2.5}$$

of which its present value is conventionally expressed as $H_0 = 100h$ km s^{-1} Mpc^{-1}, where h is the dimensionless Hubble parameter and unless otherwise stated we take a value of $h = 0.743 \pm 0.043$ (Chávez et al., 2012; Freedman et al., 2012; Riess et al., 2011; Freedman et al., 2001; Tegmark et al., 2006).

The time derivative of eq.(2.3) gives:

$$\ddot{a} = \frac{8\pi G}{3}\left(\rho a + \frac{\dot{\rho}a^2}{2\dot{a}}\right) + \frac{\Lambda a}{3},$$

and from the above and eq.(2.4) we can eliminate $\ddot{a}$ to obtain

$$\begin{aligned} \frac{-4\pi G a}{3}\left[(\rho + 3p) + 2\left(\rho + \frac{\dot{\rho}a}{2\dot{a}}\right)\right] &= 0 \\ \frac{a}{\dot{a}}\dot{\rho} + 3(\rho + p) &= 0, \end{aligned}$$

which then gives:

$$\dot{\rho} + \frac{3\dot{a}}{a}(\rho + p) = 0, \tag{2.6}$$

which is an expression of energy conservation.

Equation (2.6) can be written as

$$\frac{d(\rho a^3)}{dt} = -3a^2\dot{a}p \tag{2.7}$$

$$\frac{d(\rho a^3)}{da} = -3a^2 p, \tag{2.8}$$

and thus:

$$d(\rho_i a^3) = -p_i da^3, \tag{2.9}$$

where the subscript i runs over all the components of the Universe. Equation (2.9) is the expanding universe analog of the first law of thermodynamics, $dE = -pdV$.

If we assume that the different components of the cosmological fluid have an equation of state of the generic form:

$$p_i = w_i \rho_i, \tag{2.10}$$

then from eq.(2.8) we have

$$\frac{d(\rho_i a^3)}{da} = -3w_i\rho_i a^2, \tag{2.11}$$

which in the case where the equation of state parameter depends on time, ie., $w_i(a)$, the corresponding density takes the following form:

$$\rho_i \propto \exp\left\{-3\int \frac{da}{a}[1 + w_i(a)]\right\} . \tag{2.12}$$

For the particular case where w_i is a constant through cosmic time, we have

$$\rho_i \propto a^{-3(1+w_i)}, \tag{2.13}$$

where $w_i \equiv p_i/\rho_i$.These last two equations can be written as a function of redshift, defined by the eq.(2.2), as:

$$\rho_i \propto \exp\left[3\int_0^z \frac{1+w_i(z')}{1+z'}dz'\right], \tag{2.14}$$

$$\rho_i \propto (1+z)^{3(1+w_i)}\ . \tag{2.15}$$

For the case of non-relativistic matter (dark matter and baryons), $w_m = 0$ and $\rho_m \propto (1+z)^3$, while for relativistic particles (radiation and neutrinos), $w_r = 1/3$ and $\rho_r \propto (1+z)^4$, while for vacuum energy (cosmological constant), $w_\Lambda = -1$ and for which we have $p_\Lambda = -\rho_\Lambda = -\Lambda/8\pi G$.

In general the dark energy equation of state can be parameterized as (e.g. Plionis et al., 2009)

$$p_w = w(z)\rho_w, \tag{2.16}$$

where

$$w(z) = w_0 + w_1 f(z), \tag{2.17}$$

with $w_0 = w(0)$ and $f(z)$ is an increasing function of redshift, such as $f(z) = z/(1+z)$ (Chevallier & Polarski, 2001; Linder, 2003; Peebles & Ratra, 2003; Dicus & Repko, 2004; Wang & Mukherjee, 2006).

The so called critical density corresponds to the total energy density of the Universe. From eq.(2.3), where we take the cosmological constant as a cosmic fluid, and the definition of the Hubble parameter, eq.(2.5), we have that:

$$\rho_c \equiv \frac{3H_0^2}{8\pi G} = 1.88\times10^{-29}h^2\ \text{g cm}^{-3} = 8.10\times10^{-47}h^2\ \text{GeV}^4\ . \tag{2.18}$$

This parameter provides a convenient mean to normalize the mass-energy densities of the different cosmic components, and we can write:

$$\Omega_i = \frac{\rho_i(t_0)}{\rho_c}\ , \tag{2.19}$$

where the subscript i runs over all the different components of the cosmological fluid. Using this last definition and eq.(2.14) we can write eq.(2.3) as:

$$H^2(z) = H_0^2\left[\Omega_r(1+z)^4 + \Omega_m(1+z)^3 + \Omega_k(1+z)^2 + \Omega_w \exp\left(3\int_0^z \frac{1+w(z')}{1+z'}dz'\right)\right], \tag{2.20}$$

where Ω_k has been defined as

$$\Omega_k \equiv \frac{-k}{a^2 H_0^2} \, .$$

By definition we have that $\Omega_r + \Omega_m + \Omega_k + \Omega_w \equiv 1$, and as a useful parameter we can define $\Omega_0 \equiv \Omega_r + \Omega_m + \Omega_w$, such that for a positively curved Universe $\Omega_0 > 1$ and for a negatively curved Universe $\Omega_0 < 1$.

The value of the curvature radius, $R_{curv} \equiv a/\sqrt{|k|}$, is given by

$$R_{curv} = \frac{H_0^{-1}}{\sqrt{|\Omega_0 - 1|}}, \tag{2.21}$$

then its characteristic scale or Hubble radius is given by $H_0^{-1} \approx 3000 h^{-1}$ Mpc.

2.1.1 Observational toolkit

In observational cosmology the fundamental observable is the redshift, and therefore it is important to express the distance relations in terms of z. The first distance measure to be considered is the lookback time, i.e. the difference between the age of the Universe at observation t_0 and the age of the Universe, t, when the photons were emitted. From the definitions of redshift, eq.(2.2), and the Hubble parameter, eq.(2.5), we have:

$$\frac{dz}{dt} = -\frac{\dot{a}}{a^2} = -H(z)(1+z) \, ,$$

from which we have:

$$dt = -\frac{dz}{H(z)(1+z)} \, , \tag{2.22}$$

and the lookback time is defined as:

$$t_0 - t = \int_t^{t_0} dt = \int_0^z \frac{dz'}{H(z')(1+z')} = \frac{1}{H_0} \int_0^z \frac{dz'}{(1+z')E(z')} \, , \tag{2.23}$$

where

$$E(z) = \sqrt{\Omega_r (1+z)^4 + \Omega_m (1+z)^3 + \Omega_k (1+z)^2 + \Omega_w \exp\left(3 \int_0^z \frac{1+w(z')}{1+z'} dz'\right)} \, . \tag{2.24}$$

From the definition of lookback time it is clear that the cosmological time or the time back to the Big Bang, is given by

$$t(z) = \int_z^\infty \frac{dz'}{(1+z')H(z')} \, . \tag{2.25}$$

In the following discussion it will be useful to have an adequate parameterization of the FRW metric (Hobson, Efstathiou & Lasenby, 2005) which is given by:

$$ds^2 = dt^2 - a^2(t)\left[d\chi^2 + S^2(\chi)(d\theta^2 + \sin^2\theta d\phi^2)\right],$$

where the function $r = S(\chi)$ is:

$$S(\chi) = \begin{cases} \sqrt{k}^{-1}\sin(\chi\sqrt{k}) & \text{if } k > 0, \\ \chi & \text{if } k = 0, \\ \sqrt{|k|}^{-1}\sinh(\chi\sqrt{|k|}) & \text{if } k < 0, \end{cases} \tag{2.26}$$

We can see that the comoving distance, i.e., that between two free falling particles which remains constant with epoch, is defined by:

$$\chi = \int_t^{t_0} \frac{dt}{a(t)} = \frac{1}{H_0}\int_0^z \frac{dz'}{E(z')}\,. \tag{2.27}$$

The transverse comoving distance (also called proper distance) is defined as:

$$D_M(t) = a(t)S(\chi), \tag{2.28}$$

At the present time and for the case of a flat model we have, $D_M = a(t_0)\chi = \chi$.

The angular distance is defined as the ratio of an object's physical transverse size to its angular size, and can be expressed as:

$$D_A = \frac{D_M}{1+z}\,. \tag{2.29}$$

Finally, the luminosity distance is defined by means of the relation

$$f = \frac{L}{4\pi D_L^2}, \tag{2.30}$$

where f is an observed flux, L is the intrinsic luminosity of the observed object and D_L is the luminosity distance; from which one obtains:

$$D_L = (1+z)D_M = (1+z)\int_0^z \frac{dz'}{H(z')}\,. \tag{2.31}$$

The distance modulus of a given cosmic object is defined as:

$$\mu \equiv m - M = 5\log(D_L/10\text{ pc}) \tag{2.32}$$

where m and M are the apparent and absolute magnitude of the object, respectively. If the distance, D_L, is expressed in Mpc then we have:

$$\mu = 5\log D_L + 25\,. \tag{2.33}$$

Through this relation and with the use of standard candles, i.e. objects of fixed absolute magnitude M, we can constrain the different parameters of the cosmological models via the construction of the Hubble diagram (the magnitude-redshift relation).

The following relation is useful when working with fluxes and luminosities instead of magnitudes,

$$\log L = \log f + 0.4\mu + 40.08 \,, \tag{2.34}$$

where f is the observed flux of the object, L the luminosity and μ the distance modulus as defined in 2.33.

The scale factor can be Taylor expanded around its present value:

$$\begin{aligned} a(t) &= a(t_0) - (t_0 - t)\dot{a}(t_0) + \frac{1}{2}(t_0 - t)^2\ddot{a}(t_0) - \cdots \\ &= a(t_0)[1 - (t_0 - t)H(t_0) - \frac{1}{2}(t_0 - t)^2 q(t_0)H^2(t_0) - \cdots] \\ &= 1 + H_0(t - t_0) - \frac{1}{2}q_0 H_0^2(t - t_0)^2 + \cdots \,, \end{aligned}$$

where the deceleration parameter $q(t)$ is given by

$$q(t) \equiv -\frac{\ddot{a}(t)a(t)}{\dot{a}^2(t)} \,. \tag{2.35}$$

From the previous definitions we can write an approximation to the distance-redshift relation as

$$H_0 D_L = z + \frac{1}{2}(1 - q_0)z^2 + \cdots \,, \tag{2.36}$$

where we can recognize that for $z \ll 1$ it can be written as

$$H_0 D_L \approx z, \tag{2.37}$$

which is known as the "Hubble law".

Finally the comoving volume element, as a function of redshift, can be written as:

$$\frac{dV}{dz d\Omega} = \frac{S^2(\chi)}{H(z)} \,, \tag{2.38}$$

where Ω is the solid angle.

2.1.2 Growth of structure

The accelerated expansion of the Universe affects the evolution of cosmic structures since the expansion rate influences the growth rate of the density perturbations.

The basic assumptions regarding the evolution of structure in the Universe are that the dark matter is composed of non relativistic particles, i.e it is composed of what is called cold

dark matter (CDM), and that the initial spectrum of density perturbations is nearly scale invariant, $P(k) \sim k^{n_s}$, where the spectral index is $n_s \simeq 1$, as it is predicted by inflation. With this in mind, the linear growth of small amplitude, matter density perturbations on length scales much smaller than the Hubble radius is governed by a second order differential equation, constructed by linearizing the perturbed equations of motions of a cosmic fluid element and given by:

$$\ddot{\delta_k} + 2H\dot{\delta_k} - 4\pi G\rho_m\delta_k = 0, \tag{2.39}$$

where the perturbations $\delta_k \equiv \delta\rho_m(\mathbf{x}, t)/\bar{\rho}_m(t)$ have been decomposed into their Fourier modes of wave number k. The expansion of the Universe enters through the so-called "Hubble drag" term, $2H\dot{\delta_k}$. Note that $\bar{\rho}_m$ is the mean density.

The growing mode solution of the previous differential equation, in the standard *concordance* cosmological model ($w_\Lambda = -1$) is given by:

$$\delta_k(z) \propto H(z)(5\Omega_m/2)\int_z^\infty \frac{1+z'}{H^3(z')}dz' \ . \tag{2.40}$$

From the previous equation we obtain that, $\delta_k(t)$ is approximately constant during the radiation dominated epoch, grows as $a(t)$ during the matter dominated epoch and again is constant during the cosmic acceleration dominated epoch, in which the growth of linear perturbations effectively freezes.

2.2 Empirical Evidence

The cosmic acceleration was established empirically at the end of the 1990s when two independent teams, the *Supernova Cosmology Project* and the *High-z Supernova Search*, succeeded in their attempt to measure the supernova Hubble diagram up to relatively high redshifts ($z \sim 1$) (Riess et al., 1998; Perlmutter et al., 1999). Surprisingly, both teams found that the distant supernovae are ~ 0.25 mag dimmer that they would be in a decelerating universe, indicating that the cosmic expansion has been accelerating over the past ~ 7 Gyr (see Figure 2.1).

The cosmic acceleration has been verified by many other probes, and in this section we will briefly review the current evidence on which this picture of the Universe was constructed.

2.2.1 Cosmic microwave background

The measurement of the CMB black body spectrum was one of the most important tests of the big bang cosmology. The CMB spectrum started being studied by means of balloon and rocket borne observations and finally the black body shape of the spectrum was settled in the 1990s by observations with the FIRAS radiometer at the Cosmic Background Explorer

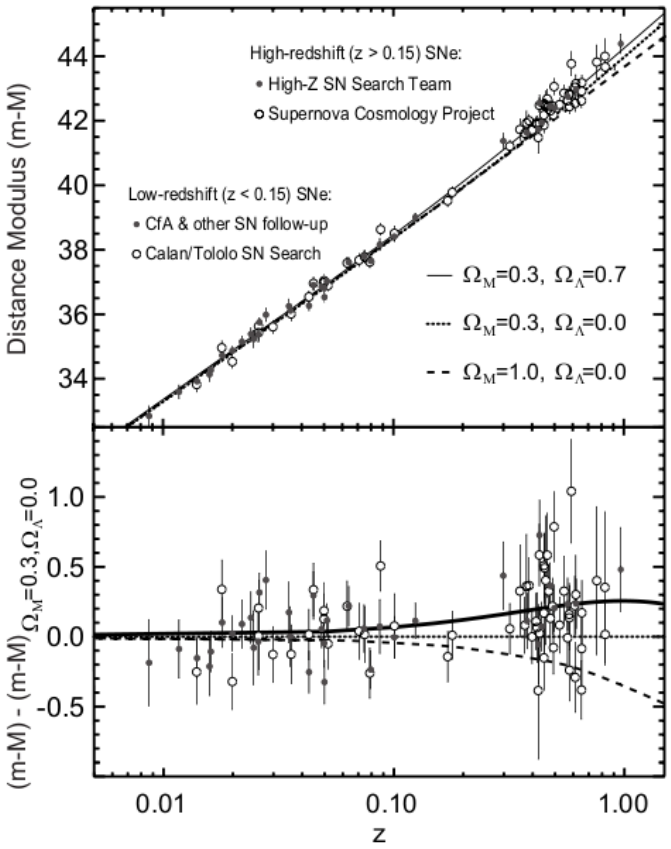

Figure 2.1: *Upper panel:* Hubble diagram of type Ia supernovae measured by the Supernova Cosmology Project and the High-z Supernova Team. *Lower Panel:* Residuals in distance modulus relative to an open Universe with $\Omega_0 = \Omega_m = 0.3$. Taken from Perlmutter & Schmidt (2003).

Satellite (COBE) (Mather et al., 1990), which also showed that the departures from a pure blackbody were extremely small ($\delta E/E \leq 10^{-4}$) (Fixsen et al., 1996).

The CMB anisotropies provide a vision of the Universe when photons decoupled from baryons and before structure developed, about 380000 years after the Big Bang. The angular power spectrum of the CMB temperature anisotropies is dominated by acoustic peaks that arise from gravity-driven sound waves in the photon-baryon fluid. The position and amplitudes of the acoustic peaks indicate it the Universe is spatially flat or not (see Figure 2.2). Furthermore, in combination with Large Scale Structure (LSS) or independent H_0 measurements, it shows that the matter contributes only about 25% of the critical energy density (Hu & Dodelson, 2002). Clearly, a component of missing energy is necessary to match both results, a fact which is fully consistent with the dark energy being an explanation of the accelerated expansion.

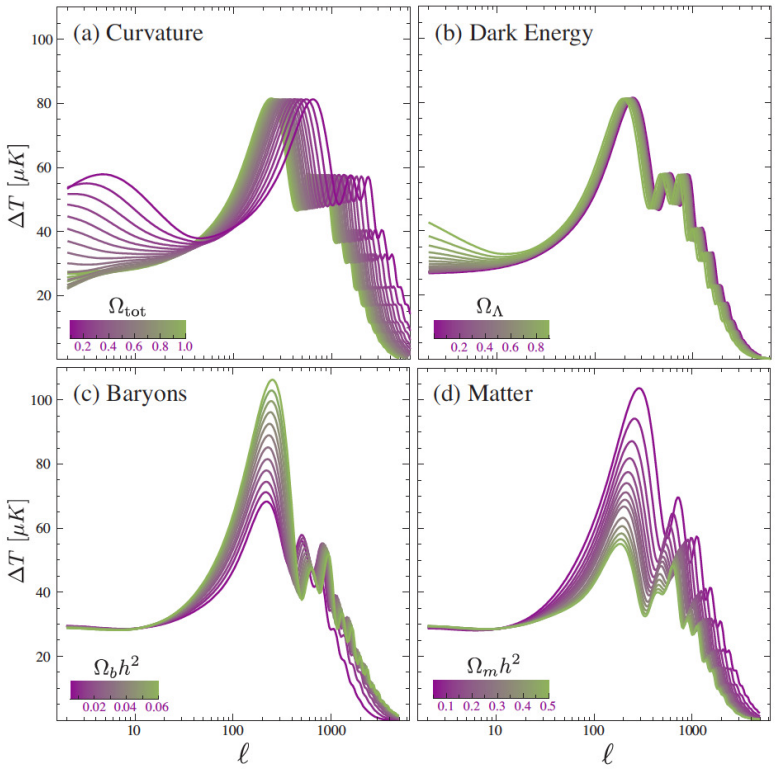

Figure 2.2: Sensitivity of the acoustic temperature spectrum to four fundamental cosmological parameters. (a) The curvature as quantified by Ω_0. (b) The dark energy as quantified by the cosmological constant Ω_Λ ($w_\Lambda = -1$). (c) The baryon density $\Omega_b h^2$. (d) The matter density $\Omega_m h^2$. All parameters are varied around a fiducial model with: $\Omega_0 = 1, \Omega_\Lambda = 0.65, \Omega_b h^2 = 0.02, \Omega_m h^2 = 0.147, n = 1, z_{ri} = 0, E_i = 0$. Taken from Hu & Dodelson (2002).

Measurements of the angular power spectrum of the CMB have been carried out in the last ten years by many experiments (e.g. Jaffe et al., 2001; Pryke et al., 2002; Spergel et al., 2007; Reichardt et al., 2009)]. Figure 2.3 shows a combination of some recent results where the first acoustic peak around $l = 200$ is clearly seen, which constrain the spatial curvature of the universe to be very close to null.

The most recent results from the Planck mission (Planck Collaboration et al., 2013) are shown in Figure 2.4. The Planck mission results are consistent with the standard spatially-flat six-parameter ΛCDM cosmology but with a slightly lower value for H_0 and a higher value for Ω_m compared with the SNe Ia results. When curvature is included, the Planck CMB data is consistent with a flat Universe to percent level precision.

Although all these results are consistent with an accelerating expansion of the universe, they alone are not conclusive; other cosmological data, like the independent measurement

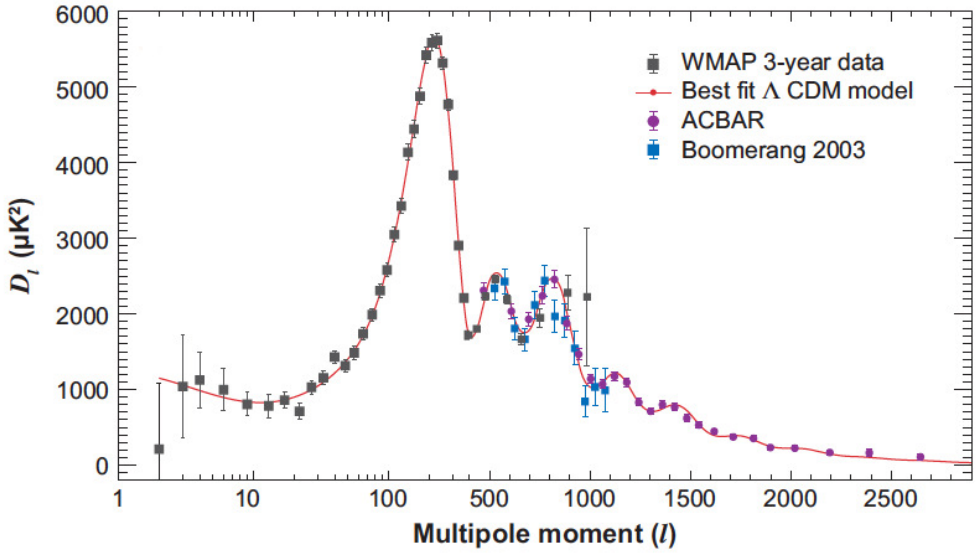

Figure 2.3: Angular power spectrum measurements of the cosmic microwave background temperature fluctuations from the Wilkinson Microwave Anisotropy Probe (WMAP), Boomerang, and the Arcminute Cosmology Bolometer Array Receiver (ACBAR). Taken from Frieman, Turner & Huterer (2008).

of the Hubble constant, are necessary in order to indicate the cosmic acceleration.

2.2.2 Large-scale structure

The two-point correlation function of galaxies, as a measure of distribution of galaxies on large scales, has long been used to provide constrains on various cosmological parameters. The measurement of the correlation function of galaxies from the APM survey excluded, at that time, the standard cold dark matter (CDM) picture (Maddox et al., 1990) and subsequently argued in favor of a model with a low density CDM and possibly a cosmological constant (Efstathiou, Sutherland & Maddox, 1990).

The baryonic acoustic oscillations (BAO) leave a characteristic signature in the clustering of galaxies, a bump in the two-point correlation function at a scale $\sim 100h^{-1}$ Mpc that can be measured today. Measurements of the BAO signature have been carried out by Eisenstein et al. (2005) for luminous red galaxies of the Sloan Digital Sky Survey (SDSS). They find results for the value of $\Omega_m h^2$ and the acoustic peak at $100h^{-1}$ Mpc scale which are consistent with the outcome of the CMB fluctuation analyses (see Figure 2.5).

The recent work by Padmanabhan et al. (2012) reanalyses the Eisenstein et al. (2005) sample using an updated algorithm to account for the effects of survey geometry as well as redshift-space distortions finding similar results, while more recently Anderson et al.

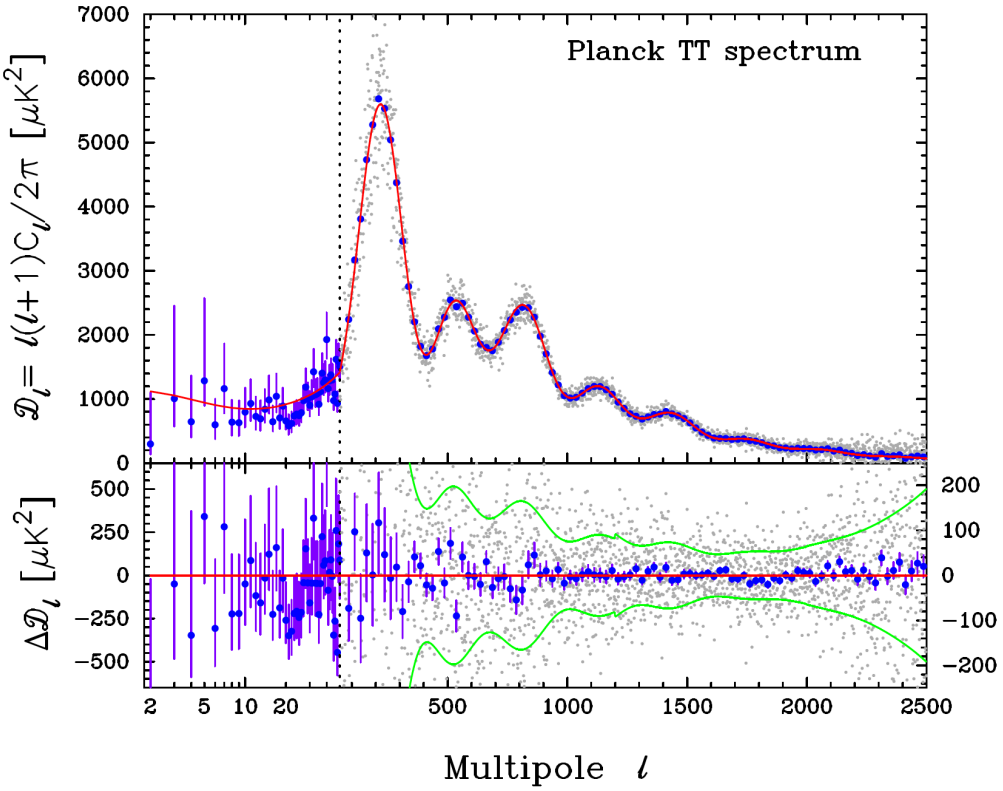

Figure 2.4: Angular power spectrum measurements of the cosmic microwave background temperature fluctuations form Planck. The power spectrum at low multipoles ($l = 2 - 49$) is plotted in a logarithmic multipole scale. Taken from Planck Collaboration et al. (2013).

(2014), using the clustering of galaxies from the SDSS DR11 and in combination with the data from Planck find best fits of $\Omega_m h^2 = 0.1418 \pm 0.0015$ and $\Omega_m = 0.311 \pm 0.009$.

2.2.3 Current supernovae results

After the first SNe Ia results were published, concerns were raised about the possibility that intergalactic extinction or evolutionary effects could be the cause of the observed distant supernovae dimming (Aguirre, 1999; Drell, Loredo & Wasserman, 2000). Since then a number of surveys have been conducted which have strengthened the evidence for cosmic acceleration. Observations with the Hubble Space Telescope (HST), have provided high quality light curves (Riess et al., 2007), and observations with ground based telescopes, have permitted the construction of two large surveys, based on 4 meter class telescopes, the SNLS (Supernova Legacy Survey) (Astier et al., 2006) and the ESSENCE (Equation of State: Supernovae Trace Cosmic Expansion) survey (Miknaitis et al., 2007) with spectroscopic

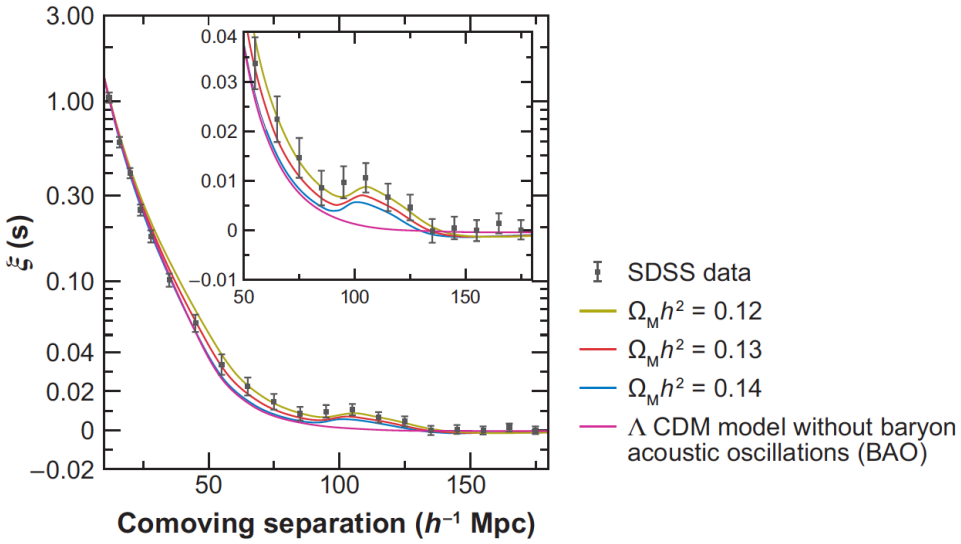

Figure 2.5: Detection of the baryon acoustic peak in the clustering of luminous red galaxies in the Sloan Digital Sky Survey (Eisenstein et al., 2005). The two-point galaxy correlation function in redshift space is shown; the inset shows an expanded view with a linear vertical axis. Curves correspond to the ΛCDM predictions for $\Omega_m h^2 = 0.12$ (dark yellow), 0.13 (red), and 0.14 (blue). The magenta curve shows a ΛCDM model without baryonic acoustic oscillations. Taken from Frieman, Turner & Huterer (2008).

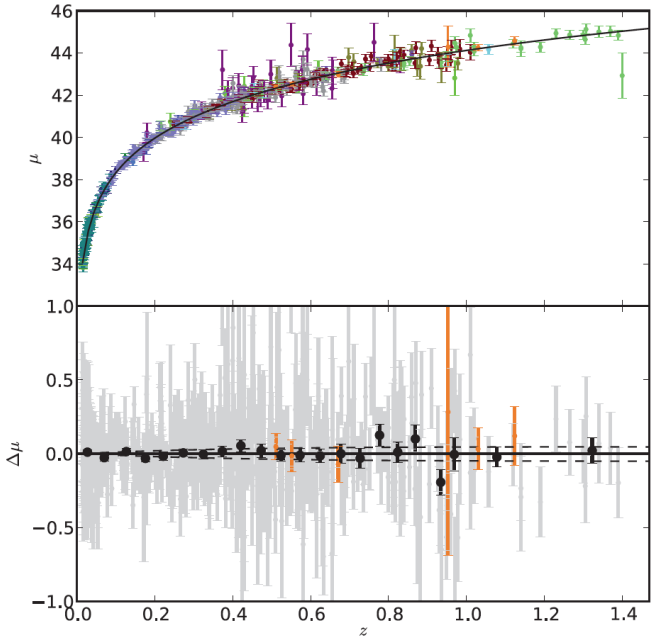

Figure 2.6: *Upper panel:* Hubble diagram for the *Union2* SNe Ia compilation. The solid line represents the best fitted cosmology for a flat Universe including CMB and BAO constraints. The different colours indicate the different data. *Lower panel:* Hubble diagram residuals where the best fitted cosmology has been subtracted from the light curve shape and color corrected peak magnitudes. The grey points show the residuals for individual SNa, while the black points show the binned values in redshifts bins of 0.05 for $z < 1.0$ and 0.2 for $z > 1.0$. The dashed lines show the expected Hubble diagram residuals for cosmological models with $w \pm 0.1$ from the best fitted value. Taken from Amanullah et al. (2010).

follow ups on larger telescopes.

The SNe Ia Hubble diagram has been constantly improved by the addition of new data, from the above mentioned surveys, mostly at $z < 1.0$. Amanullah et al. (2010) have succeeded in analyzing the current SNe Ia data (557 objects) homogeneously and have taken care of known systematics, forming what has been named the *Union2* compilation. Figure 2.6 shows the Hubble diagram based on the *Union2* dataset, where the solid line represents the best fitted cosmology, obtained from an iterative χ^2-minimization procedure based on:

$$\chi^2 = \sum_{\text{SNe}} \frac{[\mu_B(\alpha, \beta, M_B) - \mu(z; \Omega_m, \Omega_w, w)]^2}{\sigma^2_{\text{ext}} + \sigma^2_{\text{sys}} + \sigma^2_{\text{lc}}} \,, \tag{2.41}$$

where σ_{lc} is the propagated error of the covariance matrix of the light curve fit, whereas, σ_{ext} and σ_{sys} are the uncertainties associated with the Galactic extinction correction, host galaxy peculiar velocity and gravitational lensing, the former, and potential systematic

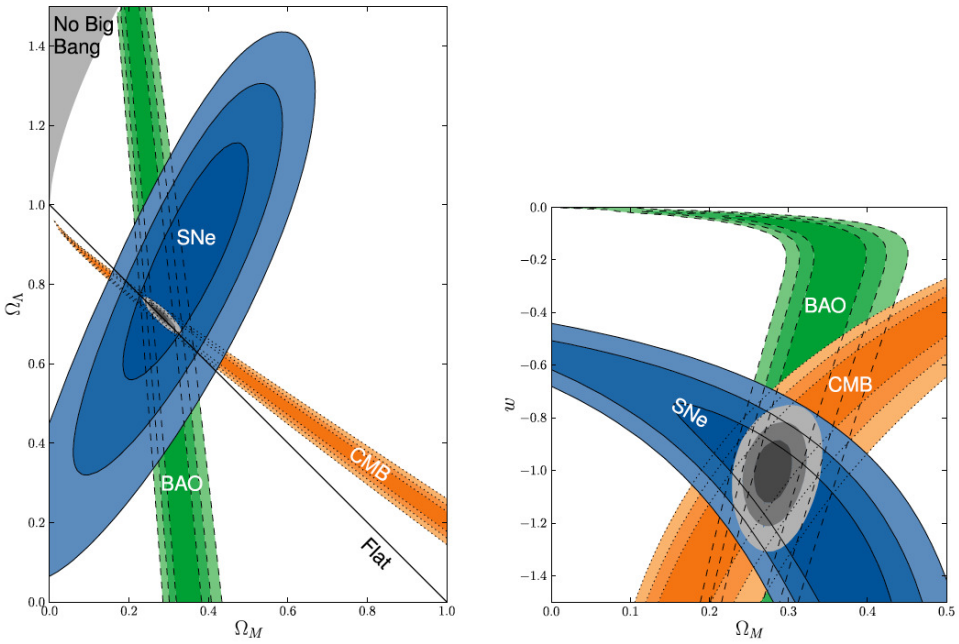

Figure 2.7: *Left panel:* 68.3 %, 95.4 % and 99.7% confidence regions in the $(\Omega_m, \Omega_\Lambda)$ plane from SNe, BAO and CMB with systematic errors. Cosmological constant dark energy ($w = -1$) has been assumed. *Right panel:* 68.3 %, 95.4 % and 99.7% confidence regions in the (Ω_m, w) plane from SNe, BAO and CMB with systematic errors. Zero curvature and constant w has been assumed. Taken from Amanullah et al. (2010).

errors the later. The observed distance modulus is defined as $\mu_B = m_B^{\rm corr} - M_B$, where M_B is the absolute B-band magnitude and $m_B^{\rm corr} = m_B^{\rm max} + \alpha x_1 - \beta c$; furthermore $m_B^{\rm max}$, x_1 and c are parameters for each supernova that are weighted by the *nuisance* parameters α, β and M_B which are fitted simultaneously with the cosmological parameters $(z; \Omega_m, \Omega_w, w)$ which give the model distance modulus μ.

Combining the data from the three probes that have been considered up to now, it is possible to obtain stronger constraints over the cosmological parameters (see Figure 2.7).

More recently, Suzuki et al. (2012) have added 23 SNe Ia (10 of which are beyond $z = 1$) to the *Union2* compilation to form the *Union2.1* dataset. Using this improved catalog of SNe Ia jointly with BAO and CMB data they obtain even better constraints to the values of the cosmological parameters as shown in Table 2.1.

2.3 Theoretical Landscape

The cosmic accelerated expansion has deep consequences for our understanding of the physical world. From the theoretical side many plausible explanations have been proposed.

Table 2.1: χ^2 minimisation results of cosmological parameters Ω_m, w and Ω_k and their uncertainties. Adapted from Suzuki et al. (2012).

Fit	Ω_m	Ω_k	w
SNe	$0.295^{+0.043}_{-0.040}$	0 (fixed)	-1 (fixed)
SNe + BAO + CMB	$0.286^{+0.018}_{-0.017}$	$-0.004^{+0.006}_{-0.007}$	-1 (fixed)
SNe + BAO + CMB + H_0	$0.272^{+0.015}_{-0.014}$	$0.002^{+0.007}_{-0.007}$	$-1.003^{+0.091}_{-0.095}$

The "simplest" one is the traditional cosmological constant, but as we will see, this solution presents serious theoretical inconsistencies. To alleviate these problems various solutions have been proposed which involve either the introduction of an exotic fluid, with negative pressure, the dynamical consequences of which evolve with time (here we call them Dark Energy theories) or a modification of general relativity.

2.3.1 The cosmological constant

The Cosmological Constant, Λ, was introduced by Einstein in his field equations, in order to obtain a static solution. It is possible since the Einstein tensor, $G^{\mu\nu} = R^{\mu\nu} - 1/2 g^{\mu\nu} R$, satisfies the Bianchi identities $\nabla_\nu G^{\mu\nu} = 0$ and the energy momentum tensor, $T^{\mu\nu}$, satisfies energy conservation $\nabla_\nu T^{\mu\nu} = 0$; furthermore the metric, $g^{\mu\nu}$, is invariant to covariant derivatives $\nabla_\alpha g^{\mu\nu} = 0$; then there is freedom to add a constant term to the GR equations:

$$R_{\mu\nu} - \frac{1}{2} g_{\mu\nu} R + \Lambda g_{\mu\nu} = 8\pi G T_{\mu\nu} \ , \tag{2.42}$$

from which we can obtain equations (2.3) and (2.4). Form eq. (2.3) we can see that:

$$\rho_\Lambda = \frac{\Lambda}{8\pi G} \ , \tag{2.43}$$

and combining the above with eq.(2.4), we can see that $p_\Lambda = -\rho_\Lambda$. As an approximation, in the case in which the energy density of the cosmological constant dominates the dynamics of the Universe, and neglecting the matter component, we have that:

$$\begin{aligned} \frac{\ddot{a}}{a} &= -\frac{4\pi G}{3}(\rho_\Lambda + 3p_\Lambda) \\ &= \frac{8\pi G}{3}\rho_\Lambda \ . \end{aligned}$$

From this rough argument, it becomes evident how the cosmological constant explains the phenomenology of the accelerated cosmic expansion, since it is clear that we have $\ddot{a} \propto \rho_\Lambda a$.

From the previous argument we see that for a cosmological constant we have $w = -1$. It is interesting to note that the current high-quality cosmological data strongly suggest that

the mechanism behind the cosmic acceleration behaves exactly as a cosmological constant. However, we will show that the Λ-based explanation of the accelerating universe presents serious theoretical inconsistencies.

From the point of view of modern field theories, the cosmological constant can be explained as the energy of the vacuum. The possible sources for the vacuum energy are basically of two kinds: a bare cosmological constant in the general relativity action or the energy density of the quantum vacuum.

The cosmological constant problem

In this subsection we introduce the cosmological constant (cc) problem or the fine tuning problem that has a long history (Weinberg, 1989), the discussion is somewhat standard (Carroll, 2001) and we roughly follow the work of Solà (2013).

A bare cosmological constant (Λ_0) can be added in the Einstein-Hilbert (EH) action:

$$S_{EH} = \frac{-1}{16\pi G}\int d^4x\sqrt{-g}(R + 2\Lambda_0) = -\int d^4x\sqrt{-g}\left(\frac{1}{16\pi G}R + \rho_{\Lambda_0}\right). \tag{2.44}$$

In fact this is the most general covariant action that we can construct from the metric and its first and second derivatives; we obtain eq.(2.42) varying this action with the addition of matter terms.

In the most simple case, the matter sector can be given by a single scalar field (ϕ). In order to trigger Spontaneous Symmetry Breaking (SSB) and then preserve the gauge symmetry of the field, we must have a potential of the form:

$$V(\phi) = \frac{1}{2}m^2\phi^2 + \frac{1}{4!}\lambda\phi^4 \ (\lambda > 0)\,, \tag{2.45}$$

where when $m^2 > 0$ we have a single vacuum state and m plays the role of a mass for the free field, whereas when $m^2 < 0$ we have two degenerate vacuum states, this situation is characteristic of a phase transition.

The action for the gravitational system including ϕ can be given as:

$$S = S_{EH} + \int d^4x\sqrt{|g|}\left[\frac{1}{2}g^{\mu\nu}\partial_\mu\phi\partial_\nu\phi - V(\phi)\right]. \tag{2.46}$$

If we transfer the bare cc term to the matter sector then the matter action is given by,

$$S[\phi] = \int d^4x\sqrt{|g|}\left[\frac{1}{2}g^{\mu\nu}\partial_\mu\phi\partial_\nu\phi - V(\phi) - \rho_{\Lambda_0}\right] = \int d^4x\sqrt{|g|}\mathcal{L}_\phi \ . \tag{2.47}$$

Calculating the energy-momentum tensor for the matter Lagrangian, as defined above, we obtain,

$$\tilde{T}^\phi_{\mu\nu} = g_{\mu\nu}\rho_{\Lambda_0} + T^\phi_{\mu\nu}\,, \tag{2.48}$$

where $T^{\phi}_{\mu\nu}$ is the scalar field energy-momentum tensor given by

$$T^{\phi}_{\mu\nu} = \left[\partial_\mu\phi\partial_\nu\phi - \frac{1}{2}g_{\mu\nu}\partial_\sigma\phi\partial^\sigma\phi\right] + g_{\mu\nu}V(\phi)\ . \tag{2.49}$$

The vacuum expectation value for the 'total' energy-momentum tensor as given in eq. (2.48) is,

$$\langle\tilde{T}^{\phi}_{\mu\nu}\rangle = g_{\mu\nu}(\rho_{\Lambda_0} + \langle V(\phi)\rangle)\ , \tag{2.50}$$

where we note that the kinematical term in eq.(2.49) does not play any role.

As said above, SBB is present when $m^2 < 0$ and then the field vacuum expected value (*vev*) is not trivial and is given by,

$$\langle\phi\rangle = \sqrt{\frac{-6m^2}{\lambda}}\ , \tag{2.51}$$

and then the *vev* for $V(\phi)$ is given by,

$$\rho_{\Lambda_i} = \langle V(\phi)\rangle = \frac{-3m^4}{2\lambda} = -\frac{1}{8}M_H^2\langle\phi\rangle^2 = \frac{-1}{8\sqrt{2}}M_H^2M_F^2\ , \tag{2.52}$$

where we have introduced M_H, the physical mass of the Higgs boson, since this is just the process that happens (at the classical level) in the electroweak phase transition generated by the Higgs potential. The value of M_H is given by,

$$M_H^2 = \left.\frac{\partial^2V(\phi)}{\partial\phi^2}\right|_{\phi=\langle\phi\rangle} = -2m^2 > 0\ . \tag{2.53}$$

Above, we also introduced the Fermi scale, $M_F = G_F^{-1/2} \simeq 293$ GeV. The value of G_F is given by

$$\frac{G_F}{\sqrt{2}} = \frac{g^2}{8M_W^2} = \frac{1}{2\langle\phi\rangle}\ , \tag{2.54}$$

where g is the weak gauge coupling and M_W is the mass of the $W^\pm$ gauge boson. Then, we have a direct measure of the Higgs *vev* given as:

$$\langle\phi\rangle = 2^{-1/4}G_F^{-1/2} \simeq 246\ \text{GeV}. \tag{2.55}$$

From eq.(2.50) it is clear that the *vev* for $V(\phi)$ plays the role of an *induced* vacuum energy, hence we have identified it in this way in eq.(2.52). At this point the physical value of the cc is given by,

$$\rho_\Lambda = \rho_{\Lambda_0} + \rho_{\Lambda_i}\ . \tag{2.56}$$

At this stage, we already can compare the above calculations with observations, combining the results in eq.(2.55) and the recently measured value for $M_H \simeq 125$ GeV (Aad et al.,

2012), we obtain a value for $\rho_{\Lambda_i} \simeq -1.2 \times 10^8$ GeV^4. The observed value of the cc is given by $\rho_\Lambda^o \sim 10^{-47}$ GeV^4, thus it is clear that,

$$\left| \frac{\rho_{\Lambda_i}}{\rho_\Lambda^o} \right| = \mathcal{O}(10^{55}) \, . \tag{2.57}$$

The last result implies that we must choose the value of ρ_{Λ_0} with a precision of 55 orders of magnitude in order to reconcile the above two results, which is clearly a severe fine-tuning problem.

The importance of the above result lies in the fact that the mass of the Higgs boson has been already measured and then at least in this, the simplest of cases, the reality of the vacuum energy density and hence the cc problem seems unavoidable.

In the most general case, and discussing the problem in a simplified way, the energy density of the quantum vacuum arises from the fact that for each mode of the quantum field there is a zero-point energy $\hbar\omega/2$. Formally the total energy would be infinite unless we discard the very high momentum modes on the ground that we trust the theory only to a certain ultraviolet momentum cutoff k_{max}, then we have

$$\rho_\Lambda = \frac{1}{2} \sum_{fields} g_i \int_0^\infty \frac{d^3k}{(2\pi)^3} \sqrt{k^2 + m^2} \simeq \sum_{fields} \frac{g_i k_{max}^4}{16\pi^3}, \tag{2.58}$$

where g_i accounts for the degrees of freedom of the field (its sign is + for bosons and − for fermions). From the last equation we can see that $\rho_\Lambda \sim k_{max}^4$, then imposing as a cutoff the energies where the known symmetry breaks, we have, in addition to the electroweak symmetry breaking discussed above, that:

- The potential arising from the breaking of chiral symmetry is due to the nonzero expectation value of the quark bilinear $q\bar{q}$ with a potential $M_{QCD} \sim 0.3$ GeV and then its contribution to the vacuum energy is $\rho_\Lambda^{QCD} \sim (0.3 \text{ GeV})^4 \sim 1.6 \times 10^{36}$ erg/cm^3.
- For the Planck scale transition we have a potential $M_{Pl} = (8\pi G)^{-1/2} \sim 10^{18}$ GeV and then its contribution to the vacuum energy is $\rho_\Lambda^{Pl} \sim (10^{18} \text{ GeV})^4 \sim 2 \times 10^{110}$ erg/cm^3.

Then, the observed value of the vacuum energy density is $10^{55} - 10^{120}$ times smaller than any theoretical prediction.

2.3.2 Dark energy theories

Due to the extreme fine tuning problem of the cc, several alternatives for the observed accelerated cosmic expansion have been proposed, a class of them postulates one or more dynamical fields with an effective value for the equation of state parameter, w, either different from -1 or changing with the redshift, in general they are called dark energy

models. Over the years many different such models have been proposed, for a recent review see Copeland, Sami & Tsujikawa (2006).

In the dark energy approach the vacuum energy, arising from the ground states of the quantum fields, has a value exactly equal to zero due to e.g. some renormalization procedure. Then the cc problem does not arise at all.

The simplest dark energy proposal is a scalar field, in general this kind of models have been named *quintessence*. The action for this model is given by

$$S = \int d^4x\sqrt{-g}\left(\frac{R}{16\pi G} + \mathcal{L}_{SM} + \mathcal{L}_Q\right), \tag{2.59}$$

where R is the Ricci scalar, g is the determinant of the metric, $\mathcal{L}_{SM}$ is the Lagrangian for Standard Model particles and the quintessence Lagrangian is given by

$$\mathcal{L}_Q = -\frac{1}{2}(\nabla_\mu Q)(\nabla^\mu Q) - V(Q)\ . \tag{2.60}$$

The field obeys the Klein-Gordon equation:

$$\Box Q = V_{,Q}; \tag{2.61}$$

and its stress-energy tensor is given by

$$T_{\mu\nu} = (\nabla_\mu Q)(\nabla_\nu Q) + g_{\mu\nu}\mathcal{L}_Q\ , \tag{2.62}$$

with energy density and pressure given by:

$$\rho_Q = \frac{1}{2}\dot{Q}^2 + V(Q), \qquad\qquad p_Q = \frac{1}{2}\dot{Q}^2 - V(Q)\ . \tag{2.63}$$

Then its equation of state parameter, $w = p/\rho$, is given by:

$$w = \frac{\dot{Q}^2/2 - V(Q)}{\dot{Q}^2/2 + V(Q)} = \frac{-1 + \dot{Q}^2/2V}{1 + \dot{Q}^2/2V}\ , \tag{2.64}$$

from which it is obvious that if the evolution of the field is slow, we have $\dot{Q}^2/2V \ll 1$, and the field behaves like a slowly varying vacuum energy, with $w < 0$, $\rho_Q(t) \propto V[Q(t)]$ and $p_Q(t) \propto -V[Q(t)]$.

2.3.3 Modified gravity theories

As it was mentioned earlier, an alternative explanation of the cosmic acceleration is through a modification to the laws of gravity. This implies a modification to the geometry side of the GR field equations, instead of the modification of the stress-energy tensor. Many ideas have been explored in this direction, some of them based on models motivated by higher-dimensional theories and string theory (e.g. Dvali, Gabadadze & Porrati, 2000; Deffayet, 2001) and others as phenomenological modifications to the Einstein-Hilbert action of GR (e.g. Carroll et al., 2004; Song, Hu & Sawicki, 2007).

2.4 Probes of Cosmic Acceleration

The accelerated expansion of the Universe appears to be a well established fact, while the dark energy density has been determined apparently to a precision of a few percent. However, measuring its equation of state parameter and determining if it is time-varying is a significantly more difficult task. The primary consequence of dark energy is its effect on the expansion rate of the universe and thus on the redshift-distance relation and on the growth-rate of cosmic structures. Therefore, we have basically two kinds of probes for dark energy, one geometrical and the other one based on the rate of growth of density perturbations.

The *Growth* probes are related to the rate of growth of matter density perturbations, a typical example being the spatial clustering of extragalactic sources and its evolution (e.g. Pouri, Basilakos & Plionis, 2014). The *Geometrical* probes are related directly to the metric, a typical example being the redshift-distance relation as traced by SNe Ia (e.g. Suzuki et al., 2012).

In general, in order to use the latter probes, based on any kind of tracers, one has to measure the redshift which is relatively straightforward, but also the tracer distance, which in general is quite difficult. In Appendix B we review the cosmic distance ladder which allows the determination of distances to remote sources.

2.4.1 Type Ia supernovae

Type Ia Supernovae have been used as geometrical probes, they are standard candles (Leibundgut, 2001), which through their determination of the Hubble function have provided constrains of cosmological parameters through eq.(2.32). Up to date they are the most effective, and better understood, probe of the cosmic acceleration (Frieman, Turner & Huterer, 2008).

The standardisation of SNe Ia became possible after the work of Phillips (1993) where an empirical correlation was established between their peak brightness and the luminosity decline rate, after peak luminosity (in the sense that more luminous SNe Ia decline more slowly).

The main systematics in the distance determination derived from SNe Ia, are uncertainties in host galaxy extinction correction and in the SNe Ia intrinsic colours, luminosity evolution and selection bias in the low redshift samples (Frieman, Turner & Huterer, 2008). The extinction correction is particularly difficult since having the combination of photometric errors, variation in intrinsic colours and host galaxy dust properties, causes distance uncertainties even when using multiband observations. However, a promising solution to this problem is based on near infrared observations, where the extinction effects are significantly reduced.

Frieman et al. (2003) estimated that in order to obtain precise measurements of w_0 and w_1, accounting for SNe Ia systematics, requires ~ 3000 light curves out to $z \sim 1.5$,

measured with great precision and careful control of the systematics.

2.4.2 Galaxy clusters

The utility of galaxy clusters as cosmological probes relies in many aspects, among which is the determination of their mass to light ratio, where its comparison with the corresponding cosmic ratio can provide the value of Ω_m (e.g. Andernach et al., 2005), the cluster masses can be also used to derive the cluster mass function to be compared with the analytic (Press-Schechter) or numerical (N-body simulations) model expectations (Basilakos, Plionis & Solà, 2009; Haiman, Mohr & Holder, 2001; Warren et al., 2006). The determination of the cluster mass can be done by means of the relation between mass and other observable, such as X-ray luminosity or temperature, cluster galaxy richness, Sunyaev-Zel'dovich effect (SZE) flux decrement or weak lensing shear, etc (Frieman, Turner & Huterer, 2008).

Frieman, Turner & Huterer (2008) give the redshift distribution of clusters selected according to some observable O, with selection function $f(O, z)$ as

$$\frac{d^2N(z)}{dzd\Omega} = \frac{r^2(z)}{H(z)} \int_0^\infty f(O, z)dO \int_0^\infty p(O|M, z)\frac{dn(z)}{dM}dM \ , \tag{2.65}$$

where $dn(z)/dM$ is the space density of dark halos in comoving coordinates and $p(O|M, z)$ is the mass-observable relation, the probability that a halo of mass M, at redshift z, is observed as a cluster with observable property O. We can see that this last equation depends on the cosmological parameters through the comoving volume element (see equation (2.38)) and the term $dn(z)/dM$ which depends on the evolution of density perturbations.

2.4.3 Baryon acoustic oscillations

Gravity drives acoustic oscillations of the coupled photon-baryon fluid in the early universe. The scale of the oscillations is given by

$$s = \int_0^{t_{rec}} c_s(1 + z)dt = \int_{z_{rec}}^\infty \frac{c_s}{H(z)}dz, \tag{2.66}$$

where c_s is the sound speed which is determined by the ratio of the baryon and photon energy densities, whereas t_{rec} and z_{rec} are the time and redshift when recombination occurred. These acoustic oscillations leave their imprint on the CMB temperature anisotropy angular power spectrum but also in the baryon mass-density distribution. From the WMAP measurements we have $s = 147 \pm 2$ Mpc. Since the oscillations scale s provides a standard ruler that can be calibrated by the CMB anisotropies, then measurements of the BAO scale in the galaxy distribution provides a geometrical probe for cosmic acceleration (Frieman, Turner & Huterer, 2008).

The systematics that could affect the BAO measurements are related to nonlinear gravitational evolution effects, scale-dependent differences between the clustering of galaxies and

of dark matter (the so-called bias) and redshift-space distortions of the clustering, which can shift the BAO features (Frieman, Turner & Huterer, 2008).

2.4.4 Weak gravitational lensing

The images of distant galaxies are distorted by the gravitational potential of foreground collapsed structures, intervening in the line of sight of the distant galaxies. This distortion can be used to measure the distribution of dark matter of the intervening structures and its evolution with time, hence it provides a probe for the effects of the accelerated expansion on the growth of structure (Frieman, Turner & Huterer, 2008).

The gravitational lensing produced by the large scale structure (LSS) can be analysed statistically by locally averaging the shapes of large numbers of distant galaxies, thus obtaining the so called cosmic shear field at any point. The angular power spectrum of shear is a statistical measure of the power spectrum of density perturbations, and is given by (Hu & Jain, 2004):

$$P_l^{\gamma}(z_s) = \int_0^{z_s} dz \frac{H(z)}{D_A^2(z)} |W(z, z_s)|^2 P_\rho \left(k = \frac{l}{D_A(z)}; z \right), \tag{2.67}$$

where l is the angular multipole of the spherical harmonic expansion, $W(z, z_s)$ is the lensing efficiency of a population of source galaxies and it is determined by the distance distributions of the source and lens galaxies, and $P_\rho(k, z)$ is the power spectrum of density perturbations.

Some systematics that could affect weak lensing measurements are, obviously, incorrect shear estimates, uncertainties in the galaxy photometric redshift estimates (which are commonly used), intrinsic correlations of galaxy shapes and theoretical uncertainties in the mass power spectrum on small scales (Frieman, Turner & Huterer, 2008).

2.4.5 H ii galaxies

H II galaxies are dwarf galaxies with a strong burst of star formation which dominates the luminosity of the host galaxy and allows it to be seen at very large distances. The $L(\mathrm{H}\beta) - \sigma$ relation of H II galaxies allows distance modulus determination for these objects and therefore the construction of the Hubble diagrams. Hence, H II galaxies can be used as geometrical probes of the cosmic acceleration.

Previous analyses (Terlevich & Melnick, 1981; Melnick et al., 1987), have shown that the H II galaxy oxygen abundance affects systematically its $L(\mathrm{H}\beta) - \sigma$ relation. The distance indicator proposed by the authors takes into account such effects (Melnick, Terlevich & Moles, 1988), and was defined as:

$$M_z = \frac{\sigma^5}{\mathrm{O/H}} \,, \tag{2.68}$$

where σ is the galaxy velocity dispersion and O/H is the oxygen abundance relative to hydrogen. From this distance indicator, the distance modulus can be calculated as: (Melnick, Terlevich & Terlevich, 2000)

$$\mu = 2.5 \log_{10} \frac{\sigma^5}{F(\mathrm{H}\beta)} - 2.5 \log_{10}(\mathrm{O/H}) - \mathrm{A}_{\mathrm{H}\beta} - 26.44, \tag{2.69}$$

where $F(\mathrm{H}\beta)$ is the observed Hβ flux and $A_{\mathrm{H}\beta}$ is the total extinction in $H\beta$.

Some possible systematics that could affect the $L(\mathrm{H}\beta) - \sigma$ relation, are related to the reddening, the age of the stellar burst, as well as the local environment and morphology.

Through the next chapter we will explore carefully the use of H II galaxies as tracers of the Hubble function and the systematics that could arise when calibrating the $L(\mathrm{H}\beta) - \sigma$ relation for these objects.

2.5 Summary

The observational evidence for the Universe accelerated expansion is now overwhelming. The best to date data from SNe Ia, BAOs, CMB and many other tracers, all accord that we are living during an epoch in which the evolution of the Universe is dominated by some sort of dark energy.

Many different models have been proposed to explain the observed dark energy. The cosmological constant is a good candidate in the sense that all current observations are consistent with it, although suffers from severe fine tuning and coincidence problems that have given place to the proposal of dynamical vacuum energy models.

In this work we will explore an alternative probe to trace the expansion history of the Universe. H II galaxies are a promising new way to explore the nature of dark energy since they can be observed to larger redshifts that many of the currently best known cosmological probes.

Appendices

Appendix A

Cosmological Field Equations

The purpose of this appendix is to derive the Cosmological Field Equations from the General Relativity (GR) Field Equations; the approach followed for the derivation is variational since this method is intuitive, easy to follow and, not the least, very powerful.

A.1 The General Relativity Field Equations

The GR Field Equations can be written as

$$R_{\mu\nu} - \frac{1}{2} g_{\mu\nu} R + \Lambda g_{\mu\nu} = -\kappa T_{\mu\nu}, \tag{A.1}$$

or alternatively as

$$R_{\mu\nu} = -\kappa \left(T_{\mu\nu} - \frac{1}{2} T g_{\mu\nu} \right) + \Lambda g_{\mu\nu}, \tag{A.2}$$

where $R_{\mu\nu}$ is the Ricci Tensor, $T_{\mu\nu}$ is the Energy-Momentum Tensor, $g_{\mu\nu}$ is the Metric Tensor, Λ is the cosmological constant and κ is a constant given by

$$\kappa = 8\pi G, \tag{A.3}$$

note that we are using units in which $c = 1$.

Our general approach to obtain the GR field equations for the FRW metric will be simply to obtain variationaly the Ricci Tensor and then to use the value of the Energy-Momentum Tensor for a perfect fluid to obtain the right-hand side of the GR field equations.

A.2 The Euler-Lagrange Equations

From the calculus of variations we know that if we want to find a function that makes an integral dependent on that function stationary, on a certain interval, we can proceed as

follows; first we have the integral that we want to make stationary

$$S = \int_a^b L(q^a, \dot{q}^a, t)dt, \tag{A.4}$$

where we define S as the action, L is the Lagrangian which is dependent on q^a, a set of generalized coordinates (a is an index running over all the elements of the set), $\dot{q}^a$, the set of the generalized coordinates time derivatives, $\dot{q}^a \equiv dq^a/dt$ and t, the time, a parameter.

The variation of the action can be written as

$$\begin{aligned} \delta S &= \int_a^b \left(\frac{\partial L}{\partial q^a}\delta q^a + \frac{\partial L}{\partial \dot{q}^a}\delta \dot{q}^a \right) dt & \text{(A.5)} \\ &= \int_a^b \frac{\partial L}{\partial q^a}\delta q^a dt + \int_a^b \frac{\partial L}{\partial \dot{q}^a}\delta \dot{q}^a dt, & \text{(A.6)} \end{aligned}$$

integrating the last term by parts and requiring the variation δS to be zero (the condition for S to be stationary), we have

$$\begin{aligned} \int_a^b \frac{\partial L}{\partial q^a}\delta q^a dt + \left[\frac{\partial L}{\partial \dot{q}^a}\delta q^a\right]_a^b - \int_a^b \frac{d}{dt}\left(\frac{\partial L}{\partial \dot{q}^a}\right)\delta q^a dt &= 0 & \text{(A.7)} \\ \left[\frac{\partial L}{\partial \dot{q}^a}\delta q^a\right]_a^b + \int_a^b \left[\frac{\partial L}{\partial q^a} - \frac{d}{dt}\left(\frac{\partial L}{\partial \dot{q}^a}\right)\right]\delta q^a dt &= 0, & \text{(A.8)} \end{aligned}$$

since a and b are fixed then the first term vanishes and in order for the integral to be zero, since δq^a is arbitrary, then

$$\frac{d}{dt}\left(\frac{\partial L}{\partial \dot{q}^a}\right) - \frac{\partial L}{\partial q^a} = 0 \tag{A.9}$$

These are the Euler-Lagrange equations that must be satisfied in order to make the action stationary.

A.3 Variational Method for Geodesics

In order to obtain the equations for the geodesics, and from them read out the metric connection coefficients, we must solve the Euler-Lagrange equations for the Lagrangian

$$L = \frac{1}{2} g_{ab}\dot{x}^a \dot{x}^b, \tag{A.10}$$

where g_{ab} are the metric elements and $\dot{x}^a$ are the coordinates time derivatives. Applying the Euler-Lagrange equations over the Lagrangian we obtain

$$\frac{d}{dt}(g_{ac}\dot{x}^a) - \frac{1}{2}(\partial_c g_{ab})\dot{x}^a\dot{x}^b = 0 \tag{A.11}$$

$$\dot{g}_{ac}\dot{x}^a + g_{ac}\ddot{x}^a - \frac{1}{2}(\partial_c g_{ab})\dot{x}^a\dot{x}^b = 0 \tag{A.12}$$

$$(\partial_b g_{ac})\dot{x}^a\dot{x}^b + g_{ac}\ddot{x}^a - \frac{1}{2}(\partial_c g_{ab})\dot{x}^a\dot{x}^b = 0 \tag{A.13}$$

$$g_{ac}\ddot{x}^a + (\partial_b g_{ac})\dot{x}^a\dot{x}^b - \frac{1}{2}(\partial_c g_{ab})\dot{x}^a\dot{x}^b = 0, \tag{A.14}$$

since $\dot{x}^a$ and $\dot{x}^b$ commutes, then we have

$$g_{ac}\ddot{x}^a + \frac{1}{2}(\partial_b g_{ac} + \partial_a g_{bc} - \partial_c g_{ab})\dot{x}^a\dot{x}^b = 0 \tag{A.15}$$

$$g^{dc}[\ddot{x}^a + \frac{1}{2}(\partial_b g_{ac} + \partial_a g_{bc} - \partial_c g_{ab})\dot{x}^a\dot{x}^b] = 0 \tag{A.16}$$

$$\ddot{x}^d + \frac{1}{2}g^{dc}(\partial_b g_{ac} + \partial_a g_{bc} - \partial_c g_{ab})\dot{x}^a\dot{x}^b = 0 \tag{A.17}$$

$$\ddot{x}^d + \Gamma^d_{ab}\dot{x}^a\dot{x}^b = 0 \tag{A.18}$$

$$\ddot{x}^a + \Gamma^a_{bc}\dot{x}^b\dot{x}^c = 0, \tag{A.19}$$

where Γ^a_{bc} are the metric connection coefficients and were clearly defined as

$$\Gamma^a_{bc} = \frac{1}{2}g^{dc}(\partial_b g_{ac} + \partial_a g_{bc} - \partial_c g_{ab}) \tag{A.20}$$

and from (A.17) we can read without effort the metric connection coefficients.

A.4 Application to the FRW Metric

Using the FRW metric a distance element can be written as

$$ds^2 = dt^2 - a^2(t)\left[\frac{dr^2}{1-kr^2} + r^2(d\theta^2 + \sin^2\theta d\phi^2)\right] \tag{A.21}$$

then the metric is given by

$$[g_{ab}] = \begin{pmatrix} 1 & 0 & 0 & 0 \\ 0 & -\frac{a^2(t)}{1-kr^2} & 0 & 0 \\ 0 & 0 & -a^2(t)r^2 & 0 \\ 0 & 0 & 0 & -a^2(t)r^2\sin^2\theta \end{pmatrix}. \tag{A.22}$$

From the previous section, equation (A.14) is the easiest to use; then we will apply this equation successively for values of the index c running from 0 to 3. In the case in which $c = 0$ we have

$$g_{00}\ddot{x}^0 - \frac{1}{2}[(\partial_0 g_{11})\dot{x}^1\dot{x}^1 + (\partial_0 g_{22})\dot{x}^2\dot{x}^2 + (\partial_0 g_{33})\dot{x}^3\dot{x}^3] = 0, \tag{A.23}$$

then substituting and solving we obtain

$$\ddot{t} + \frac{a\dot{a}}{1-kr^2}(\dot{r})^2 + a\dot{a}r^2(\dot{\theta})^2 + a\dot{a}r^2\sin^2\theta(\dot{\phi})^2 = 0, \tag{A.24}$$

from here we can read the metric connection coefficients

$$\Gamma^0_{11} = \frac{a\dot{a}}{1-kr^2} \tag{A.25}$$

$$\Gamma^0_{22} = a\dot{a}r^2 \tag{A.26}$$

$$\Gamma^0_{33} = a\dot{a}r^2\sin^2\theta. \tag{A.27}$$

For the case when $c = 1$ we have

$$g_{11}\ddot{x}^1 + (\partial_0 g_{11})\dot{x}^1\dot{x}^0 + (\partial_1 g_{11})\dot{x}^1\dot{x}^1 - \frac{1}{2}[(\partial_1 g_{11})\dot{x}^1\dot{x}^1 + (\partial_1 g_{22})\dot{x}^2\dot{x}^2 + (\partial_1 g_{33})\dot{x}^3\dot{x}^3] = 0, \tag{A.28}$$

then substituting and solving we obtain

$$\ddot{r} + 2\frac{\dot{a}}{a}\dot{t}\dot{r} + \frac{kr}{1-kr^2}(\dot{r})^2 - r(1-kr^2)(\dot{\theta})^2 - r(1-kr^2)\sin^2\theta(\dot{\phi})^2 = 0, \tag{A.29}$$

from here we can read the metric connection coefficients

$$\Gamma^1_{01} = \frac{\dot{a}}{a} \tag{A.30}$$

$$\Gamma^1_{11} = \frac{kr}{1-kr^2} \tag{A.31}$$

$$\Gamma^1_{22} = -r(1-kr^2) \tag{A.32}$$

$$\Gamma^1_{33} = -r(1-kr^2)\sin^2\theta. \tag{A.33}$$

For the case when $c = 2$ we have

$$g_{22}\ddot{x}^2 + (\partial_0 g_{22})\dot{x}^2\dot{x}^0 + (\partial_1 g_{22})\dot{x}^2\dot{x}^1 - \frac{1}{2}(\partial_2 g_{33})\dot{x}^3\dot{x}^3 = 0, \tag{A.34}$$

then substituting and solving we obtain

$$\ddot{\theta} + 2\frac{\dot{a}}{a}\dot{\theta}\dot{t} + 2\frac{1}{r}\dot{\theta}\dot{r} - \sin\theta\cos\theta(\dot{\phi})^2 = 0, \tag{A.35}$$

from here we can read the metric connection coefficients

$$\Gamma^2_{02} = \frac{\dot{a}}{a} \tag{A.36}$$

$$\Gamma^2_{12} = \frac{1}{r} \tag{A.37}$$

$$\Gamma^2_{33} = -\sin\theta\cos\theta. \tag{A.38}$$

For the case when $c = 3$ we have

$$g_{33}\ddot{x}^3 + (\partial_0 g_{33})\dot{x}^3\dot{x}^0 + (\partial_1 g_{33})\dot{x}^3\dot{x}^1 + (\partial_2 g_{33})\dot{x}^3\dot{x}^2 = 0, \tag{A.39}$$

then substituting and solving we obtain

$$\ddot{\phi} + 2\frac{\dot{a}}{a}\dot{\phi}\dot{t} + 2\frac{1}{r}\dot{\phi}\dot{r} + 2\frac{\cos\theta}{\sin\theta}\dot{\phi}\dot{\theta} = 0, \tag{A.40}$$

from here we can read the metric connection coefficients

$$\Gamma^3_{03} = \frac{\dot{a}}{a} \tag{A.41}$$

$$\Gamma^3_{12} = \frac{1}{r} \tag{A.42}$$

$$\Gamma^3_{23} = \frac{\cos\theta}{\sin\theta} = \cot\theta. \tag{A.43}$$

A.5 Obtaining the Ricci Tensor

Having the metric connection coefficients, the next step is to obtain the independent values of the Ricci tensor which is given by

$$R_{\mu\nu} = \partial_\nu\Gamma^\sigma_{\mu\sigma} - \partial_\sigma\Gamma^\sigma_{\mu\nu} + \Gamma^\rho_{\mu\sigma}\Gamma^\sigma_{\rho\nu} - \Gamma^\rho_{\mu\nu}\Gamma^\sigma_{\rho\sigma}. \tag{A.44}$$

From the metric connection coefficients we obtain that

$$R_{00} = 3\partial_0\Gamma^1_{01} + 3(\Gamma^1_{01})^2 \tag{A.45}$$

$$= 3\left[\left(\frac{\ddot{a}}{a} - \left(\frac{\dot{a}}{a}\right)^2\right) + \left(\frac{\dot{a}}{a}\right)^2\right] \tag{A.46}$$

$$= 3\frac{\ddot{a}}{a}, \tag{A.47}$$

for R_{11} we obtain

$$R_{11} = 2\partial_1\Gamma^2_{12} - \partial_0\Gamma^0_{11} - \Gamma^0_{11}\Gamma^1_{01} - 2\Gamma^1_{11}\Gamma^2_{12} + 2(\Gamma^2_{12})^2 \tag{A.48}$$

$$= -\frac{2}{r^2} - \frac{(\dot{a}^2 + a\ddot{a})}{1-kr^2} - \frac{\dot{a}^2}{1-kr^2} - \frac{2k}{1-kr^2} + \frac{2}{r^2} \tag{A.49}$$

$$= -\frac{a\ddot{a} + 2\dot{a}^2 + 2k}{1-kr^2}, \tag{A.50}$$

for R_{22} we have

$$\begin{aligned} R_{22} &= \partial_2\Gamma^3_{23} - \partial_0\Gamma^0_{22} - \partial_1\Gamma^1_{22} + 2\Gamma^0_{22}\Gamma^2_{02} + 2\Gamma^1_{22}\Gamma^2_{12} + (\Gamma^3_{23})^2 && \text{(A.51)}\\ &\quad -3\Gamma^0_{22}\Gamma^1_{01} - \Gamma^1_{22}\Gamma^1_{11} - 2\Gamma^1_{22}\Gamma^2_{12} \\ &= -\csc^2\theta - r^2(\dot{a}^2 + \ddot{a}a) + (1-kr^2) - 2kr^2 + 2r^2\dot{a}^2 && \text{(A.52)}\\ &\quad -2(1-kr^2) + \cot^2\theta - 3r^2\dot{a}^2 + kr^2 + 2(1-kr^2) \\ &= -r^2(a\ddot{a} + 2\dot{a}^2 + 2k), && \text{(A.53)} \end{aligned}$$

finally for R_{33} we have

$$\begin{aligned} R_{33} &= -\partial_0\Gamma^0_{33} - \partial_1\Gamma^1_{33} - \partial_2\Gamma^2_{33} + 2\Gamma^0_{33}\Gamma^3_{03} + 2\Gamma^1_{33}\Gamma^3_{13} + 2\Gamma^2_{33}\Gamma^3_{23} && \text{(A.54)}\\ &\quad -3\Gamma^0_{33}\Gamma^1_{01} - \Gamma^1_{33}\Gamma^1_{11} - 2\Gamma^1_{33}\Gamma^2_{12} - \Gamma^2_{33}\Gamma^3_{23} \\ &= -r^2\sin^2\theta(\dot{a}^2 + a\ddot{a}) - 3kr^2\sin^2\theta + \sin^2\theta + \cos^2\theta - \sin^2\theta && \text{(A.55)}\\ &\quad +2r^2\sin^2\theta\dot{a}^2 - 2\sin^2\theta(1-kr^2) - 2\cos^2\theta - 3r^2\sin^2\theta\dot{a}^2 \\ &\quad +kr^2\sin^2\theta + 2\sin^2\theta(1-kr^2) + \cos\theta \\ &= -r^2\sin^2\theta(a\ddot{a} + 2\dot{a}^2 + 2k) && \text{(A.56)} \end{aligned}$$

A.6 The Energy-Momentum Tensor

In order to simplify we will assume that the matter that fills the Universe can be characterized as a perfect fluid, this assumption implies that we are neglecting any shear-viscous, bulk-viscous and heat-conductive properties of the matter (Hobson, Efstathiou & Lasenby, 2005). The energy-momentum tensor is given by

$$T^{\mu\nu} = (\rho + p)u^\mu u^\nu - pg^{\mu\nu}. \tag{A.57}$$

Since in a comoving coordinate system the 4-velocity is given simply by $u^\mu = \delta^\mu_0$ and $u_\mu = \delta^0_\mu$, then we have

$$T_{\mu\nu} = (\rho + p)\delta^0_\mu\delta^0_\nu - pg_{\mu\nu}. \tag{A.58}$$

For the contracted energy-momentum tensor we have

$$\begin{aligned} T &= T^\mu_\mu && \text{(A.59)}\\ &= (\rho + p) - p\delta^\mu_\mu && \text{(A.60)}\\ &= \rho + p - 4p && \text{(A.61)}\\ &= \rho - 3p, && \text{(A.62)} \end{aligned}$$

then, we have that

$$\begin{aligned} T_{\mu\nu} - \frac{1}{2}Tg_{\mu\nu} &= (\rho + p)\delta^0_\mu\delta^0_\nu - pg_{\mu\nu} - \frac{1}{2}(\rho - 3p)g_{\mu\nu} && \text{(A.63)}\\ &= (\rho + p)\delta^0_\mu\delta^0_\nu - \frac{1}{2}(\rho + p)g_{\mu\nu}, && \text{(A.64)} \end{aligned}$$

from here we can substitute in the right hand side of (A.2) to obtain

$$-\kappa(T_{00}-\frac{1}{2}Tg_{00})+\Lambda g_{00} = -\frac{1}{2}\kappa(\rho+3p)+\Lambda \quad (A.65)$$

$$-\kappa(T_{11}-\frac{1}{2}Tg_{11})+\Lambda g_{11} = -\left[\frac{1}{2}(\rho-p)+\Lambda\right]\frac{a^2}{1-kr^2} \quad (A.66)$$

$$-\kappa(T_{22}-\frac{1}{2}Tg_{22})+\Lambda g_{22} = -\left[\frac{1}{2}(\rho-p)+\Lambda\right]a^2r^2 \quad (A.67)$$

$$-\kappa(T_{33}-\frac{1}{2}Tg_{33})+\Lambda g_{33} = -\left[\frac{1}{2}(\rho-p)+\Lambda\right]a^2r^2\sin^2\theta. \quad (A.68)$$

A.7 The Cosmological Field Equations

In the two previous sections we have derived both sides of the GR Field Equations, then at this point the reamaining step is to combine these results to obtain the Cosmological Field Equations. For R_{00} we have

$$3\frac{\ddot{a}}{a} = -\frac{1}{2}\kappa(\rho+3p)+\Lambda \quad (A.69)$$

$$3\frac{\ddot{a}}{a} = -\frac{8\pi G}{2}(\rho+3p)+\Lambda \quad (A.70)$$

$$\frac{\ddot{a}}{a} = -\frac{4\pi G}{3}(\rho+3p)+\frac{1}{3}\Lambda; \quad (A.71)$$

for R_{11} we have

$$-\frac{a\ddot{a}+2\dot{a}^2+2k}{1-kr^2} = -\left[\frac{1}{2}\kappa(\rho-p)+\Lambda\right]\frac{a^2}{1-kr^2} \quad (A.72)$$

$$a\ddot{a}+2\dot{a}^2+2k = (4\pi G(\rho-p)+\Lambda)a^2, \quad (A.73)$$

substituting the value for $\ddot{a}$ from (A.71) we have

$$-\frac{4\pi G}{3}(\rho+3p)a^2+\frac{1}{3}\Lambda a^2+2\dot{a}^2+2k = 4\pi G(\rho-p)a^2+\Lambda a^2 \quad (A.74)$$

$$2\dot{a}^2 = \frac{4\pi G}{3}(4\rho)a^2+\frac{2}{3}\Lambda a^2-2k \quad (A.75)$$

$$\left(\frac{\dot{a}}{a}\right)^2 = \frac{8\pi G\rho}{3}-\frac{k}{a^2}+\frac{\Lambda}{3}; \quad (A.76)$$

for R_{22} we have

$$-r^2(a\ddot{a}+2\dot{a}^2+2k) = -\left[\frac{1}{2}\kappa(\rho-p)+\Lambda\right]a^2r^2 \quad (A.77)$$

$$a\ddot{a}+2\dot{a}^2+2k = (4\pi G(\rho-p)+\Lambda)a^2, \quad (A.78)$$

we have obtained (A.73), then the equation given by R_{22} is not independent. For R_{33} we have

$$-r^2\sin^2\theta(a\ddot{a}+2\dot{a}^2+2k) = -\left[\frac{1}{2}\kappa(\rho-p)+\Lambda\right]a^2r^2\sin^2\theta \quad (A.79)$$

$$a\ddot{a}+2\dot{a}^2+2k = (4\pi G(\rho-p)+\Lambda)a^2, \quad (A.80)$$

anew, we have obtained (A.73) and then the equation R_{33} is redundant.

From the previous discusion, only two of the four equations are independent (equation (A.71) and equation (A.76)):

$$\frac{\ddot{a}}{a} = -\frac{4\pi G}{3}(\rho+3p)+\frac{1}{3}\Lambda \quad (A.81)$$

$$\left(\frac{\dot{a}}{a}\right)^2 = \frac{8\pi G\rho}{3}-\frac{k}{a^2}+\frac{\Lambda}{3}, \quad (A.82)$$

these are the Cosmological Field Equations.

Appendix B

The Cosmic Distance Ladder

From the relation (2.30) we can see that knowing the values for the absolute luminosity L and the flux f for an object we can obtain immediately the value of the luminosity distance D_L; if we obtain D_L and z for a great number of objects we can determine an approximate value for H_0, as can be seen from (2.36), or constrain the cosmological model by means of the relation (2.31); then the knowledge of D_L is of great importance, although, the difficult problem is to determine the value of the absolute luminosity.

Conventionally, the objects used to measure distances in cosmology, are classified as primary and secondary distance indicators. The primary distance indicators are those whose absolute luminosities are measured either directly, by kinematic methods, or indirectly, by means of the association of these objects with others whose distance was measured by kinematic methods. The primary distance indicators are not bright enough to be studied at distances farther than the corresponding to values of z around 0.01. The secondary distance indicators are bright enough to be studied at larger distances and their absolute luminosities are known through their association with primary distance indicators (Weinberg, 2008); is by means of these last objects that we can constrain a cosmological model since, aside of other considerations, their value of z is large enough to make negligible the contribution of the peculiar velocities to the redshift determination.

B.1 Kinematic Methods to Distance Determinations

As already said, in cosmology the primary distance indicators are of importance as calibrators of the secondary distance indicators which can be used to constrain a cosmological model, but these primary distance indicators must be calibrated by means of distance determinations carried out by kinematic methods. Below we will briefly discuss the kinematic methods used to measure the distance to the primary distance indicators.

B.1.1 Trigonometric parallax

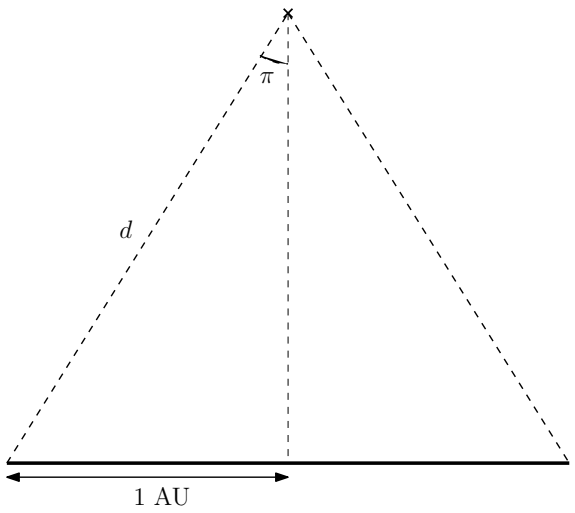

Figure B.1: Scheme illustrating the Trigonometric Parallax

While the earth's annual motion around the sun takes place, the stars appear to have an elliptical motion due to the true movement of our planet, the maximum angular radius of this motion is called parallax, π; this situation is shown schematically in Figure B.1. We can see that it is possible to calculate the actual distance to a star by means of an accurate measure of its parallax and knowing the mean distance between the sun and the earth, which is called an astronomical unit (AU). The distance to the star is given by

$$d = \frac{1 \text{ AU}}{\sin \pi}, \tag{B.1}$$

if we assume that $\pi \ll 1$ rad, which is the case for all the stars, then $\sin \pi \simeq \pi$, with enough approximation; even more, if we give π in arcseconds, we obtain the relation

$$\frac{d}{\text{pc}} = \left(\frac{\pi}{\text{arcsec}}\right)^{-1}, \tag{B.2}$$

where 1 parsec (pc) has been defined as the distance of an object when $\pi = 1''$ and the measure baseline is 1 AU, since 1 rad $= 206264.8''$ and 1 AU $= 1.49 \times 10^{13}$ cm, then

$$1 \text{ pc} = 206264.8 \text{ AU} = 3.09 \times 10^{18} \text{ cm}.$$

This simple trigonometric method can not be applied accurately from the earth surface for stars with $\pi < 0.03''$ due to atmospheric turbulence effects (seeing) which blurs the star's image; then using ground-based telescopes this method can only be used to measure distances to stars that are about 30 pc from us (Weinberg, 2008).

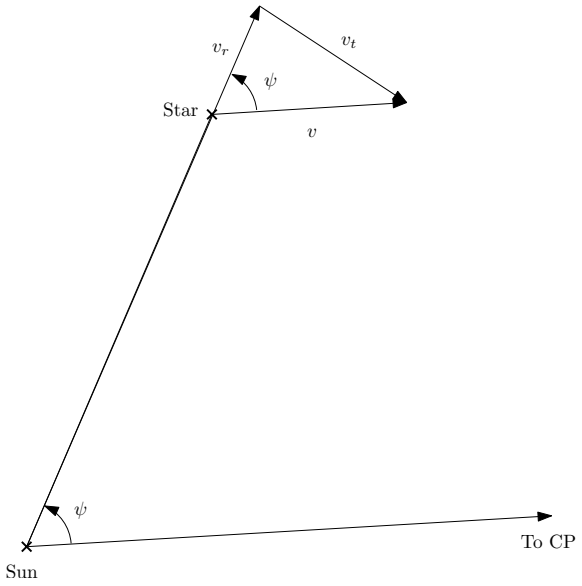

Figure B.2: Scheme that shows the geometric construction for the moving-cluster method; adapted from Binney & Merrifield (1998).

From 1989 to 1993 the Hipparcos satellite, launched by the European Space Agency (ESA), measured parallaxes for more than 100 000 stars in the solar neighbourhood with a median accuracy of $\sigma = 0.97$ mas (Perryman et al., 1997); this remarkable accuracy can be obtained since the observations were carried out from space and the usual problems related with the terrestrial atmosphere and gravitational field were not present.

B.1.2 The moving-cluster method

The fundamental assumption over which this method is constructed is that of the parallelism in the space motion of the member stars of an open cluster; i.e, the space velocity vectors of the members of the cluster, must point in the same direction. The implications of the previous assumption are that the random motions, the expansion or contraction velocities and the space velocities due to rotation, for the individual members, must be negligible (Hanson, 1975).

Since the space velocity vectors of all the stars in the cluster are parallel, then for an observer for whom the cluster is receding (or approaching), all the stars appear to be moving to (from) a convergent point (CP), the geometry for this situation is depicted in Figure B.2. From the figure we can see that the angle between the positions of the stars and the CP on the sky ψ[1], and the angle between the star's space velocity vector and the

[1]Note that this angle is seen by an outside fixed observer, from the point of view of an observer on one of the stars there is no such CP at all.

Sun-star line of sight are the same, then we have that

$$v_t = v_r \tan\psi, \tag{B.3}$$

where v_r is the radial velocity, i.e the space velocity vector component in the direction of the line of sight, and v_t is the tangent velocity defined as

$$v_t = \mu d, \tag{B.4}$$

where μ is the proper motion of the star, i.e. its angular apparent motion on the sky plane, and d is the distance from the sun to the star; then from the two previous definitions we have that

$$d = \frac{v_r \tan\psi}{\mu}, \tag{B.5}$$

or using the definition (B.2)

$$\frac{\pi}{\text{mas}} = \frac{4.74}{\tan\psi}\left(\frac{v_r}{\text{km s}^{-1}}\right)^{-1}\frac{\mu}{\text{mas yr}^{-1}}. \tag{B.6}$$

From the above relation we can determine the parallax or the distance to every star member of the cluster under consideration, using its observed proper motion, radial velocity (easily obtained measuring the shift of spectral lines) and its value of ψ (Binney & Merrifield, 1998).

B.2 Primary Distance Indicators

As previously pointed out, the primary distance indicators are of importance in the calibration of the secondary distance indicators.

B.2.1 Cepheids

The Cepheids are one of the best known primary distance indicators. These variable stars are very bright and since they exhibit a regular variation of their luminosity with time, they are useful to measure distances outside our galaxy. In 1912 Henrietta Swan Leavitt (Leavitt & Pickering, 1912) observed that the Cepheid variables that she was studying in the Small Magellanic Cloud (SMC) have fluxes that vary as a function of the period of the variation in luminosity (Leavitt law). The Cepheids pulsation periods are from 2 to over 100 days whereas their brightness variations go from $-2 < M_V < -6$ mag (Freedman & Madore, 2010).

The basic physics behind the Leavitt law is well understood, the Stephan-Boltzmann law can be written as

$$L = 4\pi R^2 \sigma T_e^4, \tag{B.7}$$

where, L, in this case, is the bolometric luminosity, R is the star radius and T_e is the star effective temperature. Expressing the above relation in therms of magnitudes, we have

$$M_{\rm BOL} = -5 \log R - 10 \log T_e + C; \tag{B.8}$$

thereafter we can map $\log T_e$ into an observable intrinsic color like $(B-V)_o$ or $(V-I)_o$ and map the radius into an observable period using a period-mean-density relation [2], then we obtain the period-luminosity-color (PLC) relation for Cepheids as (Freedman & Madore, 2010)

$$M_V = \alpha \log P + \beta (B-V)_o + \gamma. \tag{B.9}$$

Today the slope of the Period-Luminosity (PL) relation is generally taken from the Cepheids in the Large Magellanic Cloud (LMC). The values of the PL relation given by the Hubble Space Telescope (HST) key project (Freedman et al., 2001), assuming that the LMC distance modulus is $\mu(LMC) = 18.50$ mag, are

$$M_V = -2.760[\pm 0.03](\log_{10} P - 1) - 4.218[\pm 0.02] \tag{B.10}$$

$$M_I = -2.962[\pm 0.02](\log_{10} P - 1) - 4.904[\pm 0.01], \tag{B.11}$$

where P is the period in days; but these results have been under discussion due to considerations of metallicity effects in the determinations of the LMC distance modulus (Cole, 1998; Girardi et al., 1998; Salaris, Percival & Girardi, 2003).

The calibration of the PL relation can be done by observations of galactic Cepheids, in which case trigonometric parallax determinations are generally used. Using data from Hipparcos, the PL relation has been given as (Feast & Catchpole, 1997)

$$M_V = -2.81 \log_{10} P - 1.43[\pm 0.10]. \tag{B.12}$$

Assuming the slope given by the last equation, Feast (2005) has parametrized the PL relation as

$$M_V = -2.81 \log_{10} P + \gamma, \tag{B.13}$$

where γ is the PL relation zero-point, and using four distinct methods he has obtained a mean value of $\gamma = -1.40$.

Finally, recent work points out that no significant difference exists in the slopes of the PL relation between our Galaxy and the LMC (Fouqué et al., 2007), and gives for our Galaxy

$$M_V = -2.678[\pm 0.076] \log_{10} P - 1.275[\pm 0.023] \tag{B.14}$$

$$M_I = -2.980[\pm 0.074] \log_{10} P - 1.726[\pm 0.022]; \tag{B.15}$$

[2] A relation of the type $\omega_{\rm dyn} = 2\pi/P = (GM/R^3)^{1/2} \approx (G\bar{\rho})^{1/2}$, where $\omega_{\rm dyn}$ is the dynamical frequency and is proportional to the inverse of a free fall over the distance of a stellar radius.

and for the LMC

$$M_V = -2.734[\pm 0.029] \log_{10} P - 1.348[\pm 0.007] \quad \text{(B.16)}$$
$$M_I = -2.957[\pm 0.020] \log_{10} P - 1.811[\pm 0.005]; \quad \text{(B.17)}$$

where it has been assumed that the LMC distance modulus is $\mu(LMC) = 18.40$ mag, which is consistent with recent results (Benedict et al., 2007).

B.2.2 Tip of the red giant branch method

The tip of the red giant branch (TRGB) is a technique for determining distances to nearby galaxies. This method uses the well understood (Salaris, Cassisi & Weiss, 2002) discontinuity in the luminosity function (LF) of stars evolving up the red giant branch (RGB) in old, low metallicity stellar populations that has been calibrated using Galactic globular clusters; necessary condition for its application beeing that the observed RGB LF is well populated (~ 100 stars within 1 mag form the TRGB) (Madore & Freedman, 1995).

The empirical calibration of the TRGB is typically given as:

$$M_I^{TRGB} = f([\text{Fe/H}]) + \text{ZP} \quad \text{(B.18)}$$

where, M_I^{TRGB} is the absolute magnitude for the TRGB[3], $f([\text{Fe/H}])$ is a function of the metallicity (typically a polynomial), and ZP is the calibration Zero Point. This kind of models neglect the impact of other parameters on the calibration and then induce uncertainties of order ± 0.1 mag in the determination of M_I^{TRGB} (Bellazzini, 2008).

B.3 Secondary Distance Indicators

The primary distance indicators are not sufficiently bright to be observed at $z > 0.01$, brighter objects are needed as tracers to constrain a cosmological model, these brighter objects can be galaxies or supernovae, which are as bright as galaxies. We need methods to obtain the luminosity of these objects in order to determine their distances.

B.3.1 Type Ia supernovae

Type Ia Supernovae (SNe Ia) are the result of the thermonuclear destruction of an accreting carbon-oxygen white dwarf star approaching the Chandrasekhar mass limit. Observationally, the defining characteristic of SNe Ia is the absence of H and He lines and the presence of strong Si absorption lines in their spectra.

In spite of the fact that the details of the nature of the SNe Ia explosion are still obscure, the origin of the observed light curve is relatively well understood. It is powered

[3]In this case for the Cousins' I passband, but the model is similar in other bands.

by the radioactive decay of ^{56}Ni into ^{56}Co, and then into ^{56}Fe. The SN ejecta is heated by energetic gamma rays, produced by the radioactive decay, and then radiates thermally to produce the observed light curve. Photometrically, SN Ia rises to maximum light in a period of 20 days, followed by a decline of ~ 3 mag in the following month and ~ 1 mag per month subsequently (Freedman & Madore, 2010; Wolschin, 2010).

SNe Ia are not intrinsically standard candles, but can be standardized by means of simple empirical correspondences. The first of these relations is the light-curve width–luminosity relationship (WLR) or 'Phillips relation' (Phillips, 1993); essentially SN Ia peak luminosities are strongly correlated with the width of their light curve. Furthermore, SN Ia light curves can be parametrized using a 'stretch' parameter, which stretches or contracts a template light curve to match an observed one (Perlmutter et al., 1997). As an aside, the physical origin of the Phillips relation is yet not completely clear (Kasen & Woosley, 2007; Wolschin, 2010).

Another –though poorly understood– relation is between the SNe Ia luminosity and their color B - V (Tripp, 1998; Wolschin, 2010). The two previous relationships can be applied to observed peak magnitudes m:

$$m_{\rm corr} = m + \alpha(s-1) - \beta C, \tag{B.19}$$

where the stretch-luminosity is parametrized by α, and the color-luminosity relation by β. After applying the calibration to SNe Ia measurements, precise distance estimates (to $0.12 - 0.14$ mag) can be obtained.

B.3.2 Tully-Fisher relation

Tully & Fisher (1977) proposed the existence of a correlation between the global H I line (21 cm) profile width and the absolute blue magnitude of spiral galaxies; later, after the study of the correlation of the H I width and infrared luminosity, the physical basis for this relation was understood, i.e that the 21 cm line is widened by Doppler effect, caused by the rotation of the galaxy; therefore the H I line width is an indicator of the maximum speed of rotation of the galaxy V_{rot}, which by gravity is related to the mass of the galaxy, which in turn is related to the luminosity L by the mass-luminosity ratio (Aaronson, Huchra & Mould, 1979). Roughly, we have

$$L \sim V_{rot}^4. \tag{B.20}$$

The Tully-Fisher relation, calibrated with Cepheids distances and metallicity-corrected, has been given as (Sakai et al., 2000)

$$B^c_{T,Z} = -(8.07 \pm 0.72)(\log_{10} W^c_{20} - 2.5) - (19.88 \pm 0.11) \tag{B.21}$$

$$I^c_{T,Z} = -(9.46 \pm 0.76)(\log_{10} W^c_{20} - 2.5) - (21.19 \pm 0.12), \tag{B.22}$$

where $X^c_{T,Z}$ are aperture magnitudes corrected for metallicity and Galactic and internal extinction, and W^c_{20} are the 20% line widths corrected for inclination and redshift.

B.3.3 Faber-Jackson relation

For elliptical galaxies a correlation exists that is similar to the Tully-Fisher relation, only in this case between the luminosity and the velocity dispersion. The theoretical basis for this is too the Virial theorem (Faber & Jackson, 1976). The analytical form of this relation can be given roughly as

$$L_e \sim \sigma_0^4, \tag{B.23}$$

where L_e is the luminosity inside the effective radius and σ_0 is the central velocity dispersion measured from spectral line broadening (Binney & Merrifield, 1998).

Appendix C

Statistical Techniques in Cosmology

In order to analyse the large data sets that are now available for cosmological work it is absolutely necessary the use of more and more sophisticated statistical tools. Here we present a few basic statistical techniques that are used through this work and that in general can be applied in cosmological data sets analysis. Through this appendix we closely follow the work of Verde (2010).

C.1 Bayes Theorem and Statistical Inference

The fundamental rules of probability are (hereafter $\mathcal{P}$ is the probability of an event):

1. $\mathcal{P} \geq 0$.
2. $\int_{-\infty}^{\infty} dx \mathcal{P}(x) = 1$.
3. For mutually exclusive events $\mathcal{P}(x \cup y) = \mathcal{P}(x) + \mathcal{P}(y)$.
4. For dependent events $\mathcal{P}(x \cap y) = \mathcal{P}(x)\mathcal{P}(y|x)$, where $\mathcal{P}(y|x)$ is the conditional probability of y given that x has already occurred.

from the last relation we can derive the Bayes theorem (writing $\mathcal{P}(x, y) = \mathcal{P}(y, x)$):

$$\mathcal{P}(H|D) = \frac{\mathcal{P}(H)\mathcal{P}(D|H)}{\mathcal{P}(D)} \tag{C.1}$$

where D stands for *data*, H for *hypothesis* or model, $\mathcal{P}(H|D)$ is called the *posterior*, $\mathcal{P}(D|H)$ is the *likelihood* and $\mathcal{P}(H)$ is called the *prior*.

Bayes theorem is at the base of statistical inference, let us assume that we have some already collected data set, then $\mathcal{P}(D) = 1$, and we have a model characterized by some

set of parameters $\mathbf{p}$, in general we want to know the probability distribution for the model parameters given the data $\mathcal{P}(\mathbf{p}|D)$ (from a bayesian view point as opposed to a frequentist one). However, usually we can compute accurately the likelihood which, by Bayes theorem, is related to the posterior by the prior.

One fundamental problem with the above approach is that the use of distinct priors leads to different posteriors since e.g. if we have a prior in two distinct equally valid variables, then we have a distinct probability distributions for every prior, say $\mathcal{P}(x)$ and $\mathcal{G}(y)$, then in order to transform from one distribution to the other one we have

$$\mathcal{P}(x)dx = \mathcal{G}(y)dy, \tag{C.2}$$

$$\mathcal{P}(x) = \mathcal{G}(y)\left|\frac{dy}{dx}\right|. \tag{C.3}$$

Another important concept is the marginalization procedure. If we have a multivariate distribution, say $\mathcal{P}(x, y)$ and we want to know the probability distribution $\mathcal{P}(x)$ regardless of the values of y, then we *marginalize* with respect to y:

$$\mathcal{P}(x) = \int dy \mathcal{P}(x, y). \tag{C.4}$$

C.2 Chi-square and Goodness of Fit

In order to find the model, characterized by a set of parameters $\mathbf{p}$, that better fit a given data set, we must define a merit function that quantifies the correspondence between the model and the data.

The least squares fitting is given by

$$\chi^2 = \sum_i w_i[D_i - y(x_i|\mathbf{p})]^2, \tag{C.5}$$

where D_i are the data points, $y(x_i|\mathbf{p})$ is the model and w_i are suitably defined weights. The minimum variance weight is $w_i = 1/\sigma_i^2$ where σ_i denotes the error on data point i. With these weights the least squares is called chi-square. The best fit parameters are those that minimize the χ^2.

If the data are correlated, the chi-square becomes

$$\chi^2 = \sum_{ij} [D_i - y(x_i|\mathbf{p})]Q_{ij}[D_j - y(x_j|\mathbf{p})], \tag{C.6}$$

where Q denotes the inverse of the covariance matrix.

The probability distribution for the values of χ^2 around its minimum value, is given by a χ^2 distribution for $\nu = n-m$ degrees of freedom, where n is the number of independent data points and m is the number of parameters. The probability that the value of χ^2 obtained from the fit exceeds by chance the value $\hat{\chi}$ for the *correct* model is $Q(\nu, \hat{\chi}) = 1-\Gamma(\nu/2, \hat{\chi}/2)$ where Γ is the incomplete Gamma function. Q measures the goodness of the fit.

C.3 Likelihood

If in the Bayes theorem we take $\mathcal{P}(D) = 1$ since we assume that we already have the data, and $\mathcal{P}(H) = 1$ since we ignore the prior, then estimating the likelihood we obtain the posterior. However, since we have ignored the prior then we can not give the goodness of fit or the absolute probability for a model in which case we can only obtain relative probabilities. Assuming that the data are gaussianly distributed the likelihood is given by a multi-variate Gaussian:

$$\mathcal{L} = \frac{1}{(2\pi)^{n/2}|det(C)|^{1/2}} \exp\left[-\frac{1}{2}\sum_{ij}(D-y)_i C_{ij}^{-1}(D-y)_j\right], \tag{C.7}$$

where C_{ij} is the covariance matrix.

For Gaussian distributions we have $\mathcal{L} \propto \exp[-1/2\chi^2]$ and minimizing the χ^2 is equivalent to maximizing the likelihood.

The likelihood ratio is used in order to obtain results independently of the prior, it is the comparison between the likelihood at a point and the maximum likelihood, $\mathcal{L}_{max}$. Then, a model is acceptable if the likelihood ratio,

$$\Lambda = -2\ln\left[\frac{\mathcal{L}(p)}{\mathcal{L}_{max}}\right], \tag{C.8}$$

is above a given threshold.

C.4 Fisher Matrix

The Fisher matrix allows to estimate the parameters error for a given model. It is defined as

$$F_{ij} = -\left\langle \frac{\partial^2 \ln \mathcal{L}}{\partial p_i \partial p_j} \right\rangle, \tag{C.9}$$

where the average is the ensemble average over observational data (those that would be gathered if the real Universe was given by the model).

For a parameter i the marginalized error is given by

$$\sigma_{p_i} \geq (F^{-1})_{ii}^{1/2}, \tag{C.10}$$

this last equation is the Kramer-Rao inequality that implies that the Fisher matrix always gives an optimistic estimate of the errors. This inequality is an equality only if the likelihood is Gaussian, this happens when the data are gaussianly distributed and the model depends linearly on the parameters.

C.5 Monte Carlo Methods

The methodology of Monte Carlo methods for error analysis can be described as follows. Given a measured data set D_0, we can fit some model to it and obtain a set of parameters p_0 and their errors. With the intention of exploring the errors for p_0, we assume that the fitted parameters p_0 are the *true* ones. Subsequently, we construct an ensemble of simulated sets of parameters p_i^s taking care of the observational errors associated with the data set D_0. Finally, we can construct the distribution $p_i^s - p_0$ from which we can explore the parameters error.

The Monte Carlo methods for error determinations are specially useful when complicated effects can be simulated but not described analytically by a model.

List of Figures

List of Tables

References

Aad G. et al., 2012, Physics Letters B, 716, 1

Aaronson M., Huchra J., Mould J., 1979, ApJ, 229, 1

Aguirre A., 1999, ApJ, 525, 583

Albrecht A. et al., 2006, ArXiv:astro-ph/0609591

Amanullah R. et al., 2010, ApJ, 716, 712

Andernach H., Plionis M., López-Cruz O., Tago E., Basilakos S., 2005, in Astronomical Society of the Pacific Conference Series, Vol. 329, Nearby Large-Scale Structures and the Zone of Avoidance, A. P. Fairall & P. A. Woudt, ed., pp. 289–293

Anderson L. et al., 2014, MNRAS, 441, 24

Astier P. et al., 2006, A&A, 447, 31

Basilakos S., Plionis M., Solà J., 2009, Phys. Rev. D, 80, 083511

Bellazzini M., 2008, Memorie della Societa Astronomica Italiana, 79, 440

Benedict G. F. et al., 2007, AJ, 133, 1810

Binney J., Merrifield M., 1998, Galactic Astronomy. Princeton University Press

Caldwell R. R., Kamionkowski M., 2009, Annual Review of Nuclear and Particle Science, 59, 397

Carroll S. M., 2001, Living Reviews in Relativity, 4, 1

Carroll S. M., Duvvuri V., Trodden M., Turner M. S., 2004, Phys. Rev. D, 70, 043528

Chávez R., Terlevich E., Terlevich R., Plionis M., Bresolin F., Basilakos S., Melnick J., 2012, MNRAS, 425, L56

Chávez R., Terlevich R., Terlevich E., Bresolin F., Melnick J., Plionis M., Basilakos S., 2014, MNRAS, 442, 3565

Chevallier M., Polarski D., 2001, International Journal of Modern Physics D, 10, 213

Cole A. A., 1998, ApJ, 500, L137

Conley A. et al., 2011, ApJS, 192, 1

Copeland E. J., Sami M., Tsujikawa S., 2006, International Journal of Modern Physics D, 15, 1753

Deffayet C., 2001, Physics Letters B, 502, 199

Dicus D. A., Repko W. W., 2004, Phys. Rev. D, 70, 083527

Drell P. S., Loredo T. J., Wasserman I., 2000, ApJ, 530, 593

Dvali G., Gabadadze G., Porrati M., 2000, Physics Letters B, 485, 208

Efstathiou G., Sutherland W. J., Maddox S. J., 1990, Nature, 348, 705
Eisenstein D. J. et al., 2005, ApJ, 633, 560
Faber S. M., Jackson R. E., 1976, ApJ, 204, 668
Feast M., 2005, in Astronomical Society of the Pacific Conference Series, Vol. 329, Nearby Large-Scale Structures and the Zone of Avoidance, Fairall A. P., Woudt P. A., eds., p. 241
Feast M. W., Catchpole R. M., 1997, MNRAS, 286, L1
Fixsen D. J., Cheng E. S., Gales J. M., Mather J. C., Shafer R. A., Wright E. L., 1996, ApJ, 473, 576
Fouqué P. et al., 2007, A&A, 476, 73
Freedman W. L., Madore B. F., 2010, ARA&A, 48, 673
Freedman W. L. et al., 2001, ApJ, 553, 47
Freedman W. L., Madore B. F., Scowcroft V., Burns C., Monson A., Persson S. E., Seibert M., Rigby J., 2012, ApJ, 758, 24
Frieman J. A., Huterer D., Linder E. V., Turner M. S., 2003, Phys. Rev. D, 67, 083505
Frieman J. A., Turner M. S., Huterer D., 2008, ARA&A, 46, 385
Girardi L., Groenewegen M. A. T., Weiss A., Salaris M., 1998, MNRAS, 301, 149
Haiman Z., Mohr J. J., Holder G. P., 2001, ApJ, 553, 545
Hanson R. B., 1975, AJ, 80, 379
Hobson M. P., Efstathiou G. P., Lasenby A. N., 2005, General Relativity. Cambridge University Press
Hu W., Dodelson S., 2002, ARA&A, 40, 171
Hu W., Jain B., 2004, Phys. Rev. D, 70, 043009
Hubble E., 1929, Proceedings of the National Academy of Science, 15, 168
Jaffe A. H. et al., 2001, Physical Review Letters, 86, 3475
Joyce A., Jain B., Khoury J., Trodden M., 2014, ArXiv: 1407.0059
Kasen D., Woosley S. E., 2007, ApJ, 656, 661
Leavitt H. S., Pickering E. C., 1912, Harvard College Observatory Circular, 173, 1
Leibundgut B., 2001, ARA&A, 39, 67
Linder E. V., 2003, Physical Review Letters, 90, 091301
Maddox S. J., Efstathiou G., Sutherland W. J., Loveday J., 1990, MNRAS, 242, 43P
Madore B. F., Freedman W. L., 1995, AJ, 109, 1645
Mather J. C. et al., 1990, ApJ, 354, L37
Melnick J., 2003, in Astronomical Society of the Pacific Conference Series, Vol. 297, Star Formation Through Time, Perez E., Gonzalez Delgado R. M., Tenorio-Tagle G., eds., p. 3
Melnick J., Moles M., Terlevich R., Garcia-Pelayo J.-M., 1987, MNRAS, 226, 849
Melnick J., Terlevich R., Moles M., 1988, MNRAS, 235, 297
Melnick J., Terlevich R., Terlevich E., 2000, MNRAS, 311, 629
Miknaitis G. et al., 2007, ApJ, 666, 674
Padmanabhan N., Xu X., Eisenstein D. J., Scalzo R., Cuesta A. J., Mehta K. T., Kazin

E., 2012, MNRAS, 427, 2132
Peacock J. A., Schneider P., Efstathiou G., Ellis J. R., Leibundgut B., Lilly S. J., Mellier Y., 2006, ESA-ESO Working Group on "Fundamental Cosmology". Tech. rep., ESO
Peebles P. J., Ratra B., 2003, Reviews of Modern Physics, 75, 559
Perlmutter S. et al., 1999, ApJ, 517, 565
Perlmutter S. et al., 1997, ApJ, 483, 565
Perlmutter S., Schmidt B. P., 2003, in Lecture Notes in Physics, Berlin Springer Verlag, Vol. 598, Supernovae and Gamma-Ray Bursters, K. Weiler, ed., pp. 195–217
Perryman M. A. C. et al., 1997, A&A, 323, L49
Phillips M. M., 1993, ApJ, 413, L105
Planck Collaboration et al., 2013, ArXiv: astro-ph/1303.5076
Plionis M., Terlevich R., Basilakos S., Bresolin F., Terlevich E., Melnick J., Chavez R., 2011, MNRAS, 416, 2981
Plionis M., Terlevich R., Basilakos S., Bresolin F., Terlevich E., Melnick J., Georgantopoulos I., 2009, Journal of Physics Conference Series, 189, 012032
Pouri A., Basilakos S., Plionis M., 2014, ArXiv: 1402.0964
Pryke C., Halverson N. W., Leitch E. M., Kovac J., Carlstrom J. E., Holzapfel W. L., Dragovan M., 2002, ApJ, 568, 46
Ratra B., Vogeley M. S., 2008, PASP, 120, 235
Reichardt C. L. et al., 2009, ApJ, 694, 1200
Rest A. et al., 2013, ArXiv: astro-ph/1310.3828
Riess A. G. et al., 1998, AJ, 116, 1009
Riess A. G. et al., 2011, ApJ, 730, 119
Riess A. G. et al., 2007, ApJ, 659, 98
Robertson H. P., 1935, ApJ, 82, 284
Sakai S. et al., 2000, ApJ, 529, 698
Salaris M., Cassisi S., Weiss A., 2002, PASP, 114, 375
Salaris M., Percival S., Girardi L., 2003, MNRAS, 345, 1030
Seljak U. et al., 2005, Phys. Rev. D, 71, 103515
Shafer D. L., Huterer D., 2014, Phys. Rev. D, 89, 063510
Siegel E. R., Guzmán R., Gallego J. P., Orduña López M., Rodríguez Hidalgo P., 2005, MNRAS, 356, 1117
Solà J., 2013, Journal of Physics Conference Series, 453, 012015
Song Y., Hu W., Sawicki I., 2007, Phys. Rev. D, 75, 044004
Spergel D. N. et al., 2007, ApJS, 170, 377
Spergel D. N. et al., 2003, ApJS, 148, 175
Suyu S. H. et al., 2012, ArXiv: astro-ph/1202.4459
Suzuki N. et al., 2012, ApJ, 746, 85
Tegmark M. et al., 2006, Phys. Rev. D, 74, 123507
Tegmark M. et al., 2004, Phys. Rev. D, 69, 103501
Terlevich R., Melnick J., 1981, MNRAS, 195, 839

Tripp R., 1998, A&A, 331, 815
Tully R. B., Fisher J. R., 1977, A&A, 54, 661
Verde L., 2010, in Lecture Notes in Physics, Berlin Springer Verlag, Vol. 800, Lecture Notes in Physics, Berlin Springer Verlag, G. Wolschin, ed., pp. 147–177
Wang Y., Mukherjee P., 2006, ApJ, 650, 1
Warren M. S., Abazajian K., Holz D. E., Teodoro L., 2006, ApJ, 646, 881
Weinberg S., 1989, Reviews of Modern Physics, 61, 1
Weinberg S., 2008, Cosmology. Oxford University Press
Wolschin G., ed., 2010, Lecture Notes in Physics, Berlin Springer Verlag, Vol. 800, Lectures on Cosmology Accelerated Expansion of the Universe. Springer Verlag
Yadav J., Bharadwaj S., Pandey B., Seshadri T. R., 2005, MNRAS, 364, 601